OPEN BIOLOGY

royalsocietypublishing.org/rsob

Research

Cite this article: Halova L, Connolly Y, Smith D, Petersen J, Hagan I. 2026 CDK1-Cyclin B mediated phosphorylation of PP2A-B56 on B56^{Par1}.T73T75 controls mitotic entry timing and *Schizosaccharomyces pombe* cell size. *Open Biol.* **16**: 260089.
https://doi.org/10.1098/rsob.260089

Received: 5 March 2026
Accepted: 16 June 2026

Subject Areas:
biochemistry, cellular biology, genetics

Keywords:
mitotic entry, cell size, PP2A-B56, PP1

Author for correspondence:
Lenka Halova
e-mail: lenka.halova@cruk.manchester.ac.uk

Supplementary material is available online at https://doi.org/10.6084/m9.figshare.c.8576140.

THE ROYAL SOCIETY PUBLISHING

CDK1-Cyclin B mediated phosphorylation of PP2A-B56 on B56^{Par1}.T73T75 controls mitotic entry timing and *Schizosaccharomyces pombe* cell size

Lenka Halova[1], Yvonne Connolly[2], Duncan Smith[2], Janni Petersen[3] and Iain Hagan[1]

[1]Cell Division, Cancer Research UK Manchester Institute and [2]Biological Mass Spectrometry, Cancer Research UK Manchester Institute, The University of Manchester, Manchester, UK
[3]Flinders Centre for Innovation in Cancer, Flinders University College of Medicine and Public Health, Adelaide, South Australia, Australia

LH, 0000-0002-7253-6512; JP, 0000-0003-0729-9335; IH, 0000-0002-5858-9415

Mitosis is triggered when the rising activity of CDK1-Cyclin B, amplified by the CDK1/Cdc25/Wee1 feedback loop, overcomes inhibitory signalling from Wee1 and counteracting phosphatases. CDK-opposing phosphatases PP1, PP2A-B55 and PP2A-B56 are regulators of mitosis. A screen for differentially phosphorylated sites in a *ΔPP1^{dis2}* genetic background in *Schizosaccharomyces pombe* identified phosphorylation of T73 or T75 in the regulatory B56^{Par1} subunit. The B56^{Par1}.T73T75 phosphorylation is directly mediated by CDK1-Cyclin B, and a phospho-mimetic mutation increased while a non-phosphorylatable mutation reduced PP2A-B56^{Par1} phosphatase activity. Blocking B56^{Par1}.T73T75 phosphorylation reduced cell length in unperturbed divisions from 14 to 12 µm, without causing pleiotropic defects. Therefore, blocking phosphorylation at T73T75 alone prematurely unlocked amplification of the CDK1/Cdc25/Wee1 feedback loop, advancing cells into mitosis. Signalling from T73T75 reveals for the first time that timely mitotic commitment in unperturbed cycles is mediated by PP2A-B56.

1. Introduction

During interphase, CDK1-Cyclin B activity is restrained through inhibitory phosphorylation of CDK1 by Wee1 family kinases, until Cdc25 phosphatases remove the inhibitory phosphate to enforce mitotic entry [1,2]. CDK1-Cyclin B associates with the fission yeast equivalent of the centrosome, the spindle pole body (SPB), from early G2 until Cyclin B destruction in mitosis [3–5]. CDK1-Cyclin B engages polo kinase on the SPB in a positive CDK1/Cdc25/Wee1 feedback loop 30 minutes before mitosis, activating the SPB [6–10]. Mitosis in the whole cell is triggered when the signal amplification exceeds the inhibitory impact of Wee1 and CDK-counteracting phosphatases [11–14].

The serine/threonine phosphatases PP1 and PP2A are important regulators of mitosis in *Metazoa* and fission yeast [15–17]. PP1 monomers achieve specificity by docking to regulatory proteins, which direct PP1 to substrates [18,19]. PP2A holoenzymes combine a catalytic and a scaffold subunit with one of four B-type regulatory subunits, which determine the phosphatase specificity. Of these, the B55 and B56 families have been linked to mitotic control [16,20]. All three phosphatases employ preferences for the phosphorylated residue and the surrounding amino acids (AA) and are recruited to the targets through specific

sequences that include short linear motifs (SLiMs) [15,21–27]. Bulk activities of PP1 and PP2A are inhibited during mitosis, although local activities to control phosphorylations remain [16,17,28,29].

In human cells, PP2A complexity is expanded by four genes encoding B55 subunits (*α*, *β*, *γ* and *δ*) and five genes encoding B56 subunits (*α*, *β*, *γ*, *δ* and *ε*), which utilize distinct structural folds to dictate substrate specificity [30–32]. Furthermore, alternative splicing—particularly within the B56 genes—further expands this repertoire, enabling the formation of over 100 unique heterotrimeric combinations [33,34]. The PP2A-B55 family is the main antagonist of CDK phosphorylations and contributes to the bistability of mitotic entry and exit [35–37]. PP2A-B56 and PP1 are primarily employed in local controls during mitosis, where they support microtubule-kinetochore capture, chromosome alignment and spindle assembly checkpoint (SAC) silencing [26,38,39].

By contrast to animal cells, the yeast *Schizosaccharomyces pombe* only has one *B55* gene, $B55^{pab1}$, and two *B56* paralogues, $B56^{par1}$ and $B56^{par2}$, of which $B56^{Par1}$ is the major variant [40]. This relative simplicity makes *S. pombe*, an established eukaryotic cell cycle model, ideal for investigating conserved PP2A functions in mitosis. As in animal cells, PP2A-$B55^{Pab1}$ dephosphorylates many CDK-dependent phosphorylation sites, although recent data suggest that only approximately 25% of the phosphosites can be attributed to PP2A-$B55^{Pab1}$ alone, possibly reflecting substantial redundancy between phosphatases [15]. PP2A-$B55^{Pab1}$ couples cell growth to the cell cycle via the greatwall-endosulfine switch that inactivates PP2A-$B55^{Pab1}$ at the onset of mitosis [41]. PP1 is encoded by two genes in *S. pombe*, $PP1^{dis2}$ and $PP1^{sds21}$. The major $PP1^{Dis2}$ isoform restricts the CDK1/Cdc25/Wee1 feedback loop activation on the SPB in G2 [8,42]. During mitosis, $PP1^{Dis2}$ and to a lesser extent PP2A-$B56^{Par1}$ contribute to SAC silencing [43]. All three phosphatases join forces at mitotic exit to orchestrate orderly substrates dephosphorylations [28]. As Cyclin B degrades, $PP1^{Dis2}$ auto-catalytically recovers and drives a phosphatase relay, in which $PP1^{Dis2}$ binds to and sequentially activates PP2A-$B55^{Pab1}$ and PP2A-$B56^{Par1}$. Binding assays and sequence conservation suggest that PP1 regulates PP2A-B55 and PP2A-B56 activities in a variety of signalling contexts throughout eukaryotes [28,44]. A recent systematic *in vivo* analysis of phosphorylations targeted by PP1, PP2A-B55, PP2A-B56 and the dual-specificity phosphatase CDC14 in *S. pombe* substantiated that all these phosphatases negatively regulated CDK1-Cyclin B activity [15]. Interestingly, each phosphatase targeted distinct subgroups of substrate sites that were net phosphorylated at different points during the *S. pombe* cell cycle, suggesting that these phosphorylation thresholds were important for mitotic onset.

The regulatory interplay between $PP1^{Dis2}$, PP2A-$B55^{Pab1}$ and PP2A-$B56^{Par1}$ at mitotic exit indicates that $PP1^{Dis2}$ targets a phosphorylation site on the respective PP2A holoenzymes [28]. As the regulatory subunit determines PP2A specificity, we asked whether the $PP1^{Dis2}$ target on PP2A-$B56^{Par1}$ resides within the regulatory subunit itself. Here, a screen for phosphorylation sites altered upon the removal of $PP1^{Dis2}$ in fission yeast identified T73T75 phosphorylation on $B56^{Par1}$. Mimicking T73T75 phosphorylation increased the phosphatase activity of the intact PP2A-$B56^{Par1}$ complex, while blocking phosphorylation restricted activity. Phospho-blocking mutations altered mitotic entry, leading to premature mitosis at an approximately 2 µm reduced cell size, corresponding to 15% reduction in *S. pombe* cell length. The T73T75 regulation thus represents a mechanism of mitotic entry control by PP2A-B56.

2. Results

2.1. PP2A-$B56^{Par1}$.T73T75 is phosphorylated and under $PP1^{Dis2}$ control *in vivo*

To map phosphorylation on the regulatory $B56^{Par1}$ subunit, we first optimized large-scale precipitation of $B56^{Par1}$.HA under denaturing conditions, a method that preserves phosphorylations [45] (supplementary material, figure S1A). To identify $PP1^{Dis2}$-responsive sites, we then applied these optimized conditions to precipitate $B56^{Par1}$.HA from *S. pombe* cells with or without genetic disruption of $PP1^{dis2}$ (supplementary material, figure S1B). Previous studies established that deletion of $PP1^{dis2}$ has no discernible effect on cell cycle progression in unperturbed cultures, likely owing to functional compensation by the paralogue $PP1^{Sds21}$ [46–48]. Therefore, changes in $B56^{Par1}$ phosphorylation in precipitates from $\Delta PP1^{dis2}$ cells are unlikely to reflect an altered cell-cycle distribution and would be consistent with $PP1^{Dis2}$ activity regulating the sites' dephosphorylation.

Quantitative mass spectrometry identified differential phosphorylations within the unstructured N-terminal arm (threonines 73 or 75 and serine 99) and in the core B56 domain (serine 358 or 359 and threonine 361) of $B56^{Par1}$ (figure 1A,B; supplementary material, data 1). As phosphorylation of T73 or T75 was upregulated in cells lacking $PP1^{dis2}$, these sites were selected for further investigation: both residues are flanked by Prolines, suggesting a cell cycle-dependent regulation [49], and the high level of sequence homology surrounding these sites among B56 orthologues in the *Schizosaccharomyces* species (figure 1C) as well as across other eukaryotes (figure 1D), supports the existence of a conserved regulatory site.

To validate the quantitative mass spectrometry screen results, we generated dual phospho-specific antibodies against $B56^{Par1}$.T73T75 and monitored phosphorylation levels in HA-immunoprecipitates from $B56^{par1}$.*HA* cells following ablation of individual mitotic phosphatases. Importantly, the phosphorylation was elevated in cultures which lacked $PP1^{dis2}$, but not other mitotic phosphatases (figure 1E). Combined, these results identified a new phosphorylation site on the $B56^{Par1}$ subunit, T73T75, which is under the regulation of the PP1 phosphatase, specifically the $PP1^{Dis2}$ isoform.

2.2. T73T75 phosphorylation defines a novel $PP1^{Dis2}$-dependent regulation of PP2A-$B56^{Par1}$

We next asked if $B56^{Par1}$.T73T75 was a direct $PP1^{Dis2}$ target. To assess whether PP1 can directly dephosphorylate T73T75, we purified $B56^{Par1}$.HA from *S. pombe* under denaturing conditions by HA affinity and used the purified protein as a substrate in

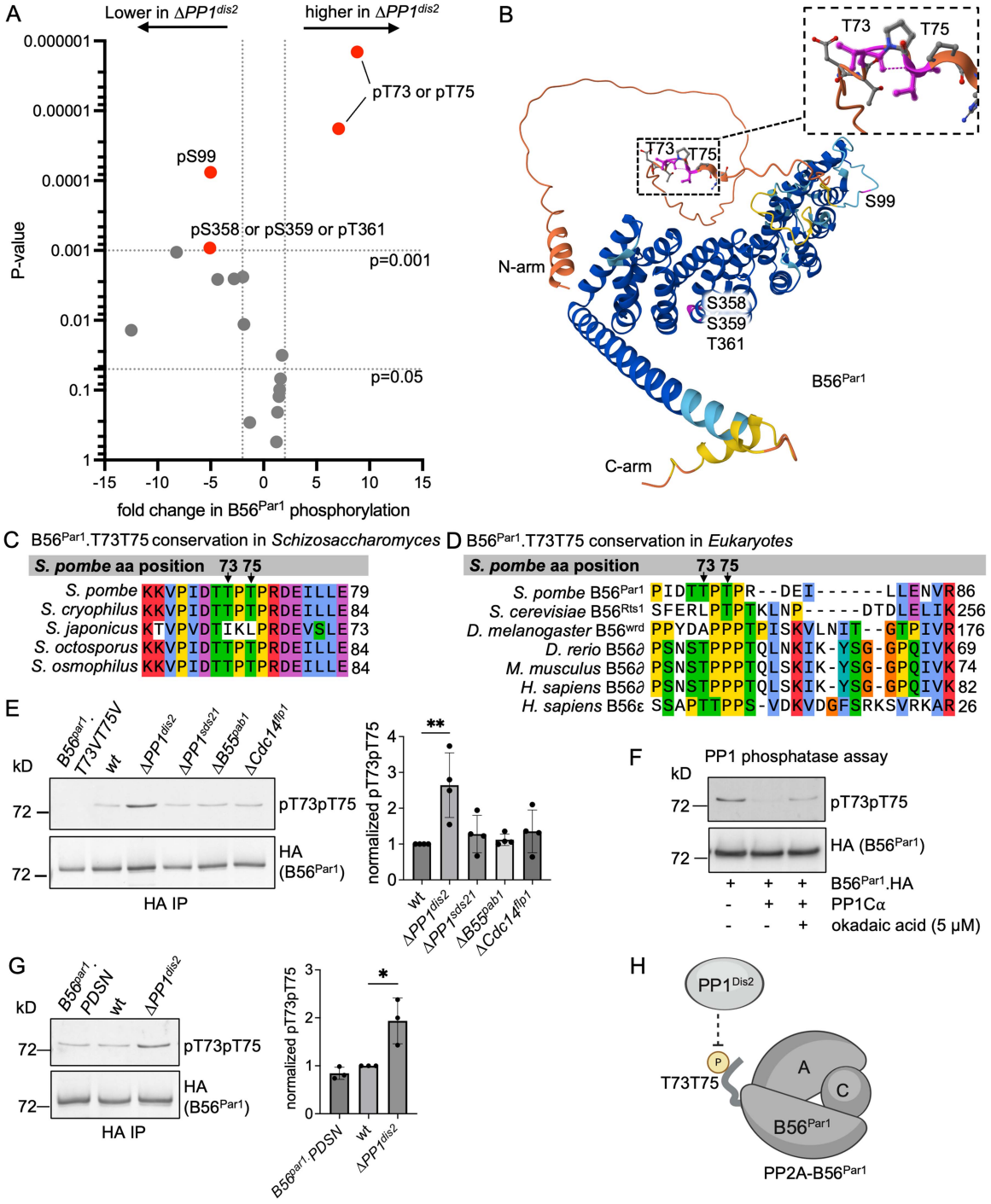

Figure 1. PP2A-B56^{Par1}.T73T75 phosphorylation is under PP1^{Dis2} control. (A) Quantitative mass spectrometry post-translational modifications (PTM) analysis of the impact of *PP1^{dis2}* ablation upon phosphorylation of B56^{Par1}. Phospho-sites changing >2 fold between wild type and Δ*PP1^{dis2}* ($p < 0.001$) are labelled in red. (B) B56^{Par1} predicted structure (source: pombase.org) with phospho-sites identified in (A) highlighted in magenta. Note that T73T75 (inset) resides in a structurally disordered N-terminal arm of B56^{Par1}. (C,D) Clustal Omega alignment of N-termini of B56 orthologues from *Schizosaccharomyces* (C) and eukaryotic (D) species. (E) B56^{Par1}.T73T75 phosphorylation levels in phosphatase-deficient mutants. Left, a representative immuno-blot; right, quantification of phosphorylation levels (means ± standard deviation (s.d.), $n = 4$). Phospho-specific signals detected with pT73pT75 phospho-specific antibodies were normalized to total levels of the B56^{Par1} target protein run on a parallel Western blot as sample processing controls, and normalized values were plotted relative to wild-type, which was set to 1. Significance was calculated by a two-way ANOVA followed by Dunnett's multiple comparisons test. $^{**}p < 0.01$. (F) Dephosphorylation of B56^{Par1}.T73T75 by PP1 in an *in vitro* phosphatase assay. pT73pT75 levels were detected by phospho-specific antibodies, and signal was developed by a chromogenic method, and the same membrane was then probed with anti-HA antibodies as a loading control with signal developed by chemiluminescence. Okadaic acid was used as a PP1 inhibitor. (G) B56^{Par1}.T73T75 phosphorylation levels in PP1 docking-site mutant *B56^{par1}.PDSN*. Left, representative immunoblot; right, quantification of levels (means ± s.d., $n = 3$) measured as in (E). $^{*}p < 0.05$. (H) Schematic depicting the control of PP2A-B56^{Par1}.T73T75 phosphorylation by PP1^{Dis2}. Dashed line represents a potentially indirect event. C, catalytic subunit; A, scaffolding subunit; wt, wild type.

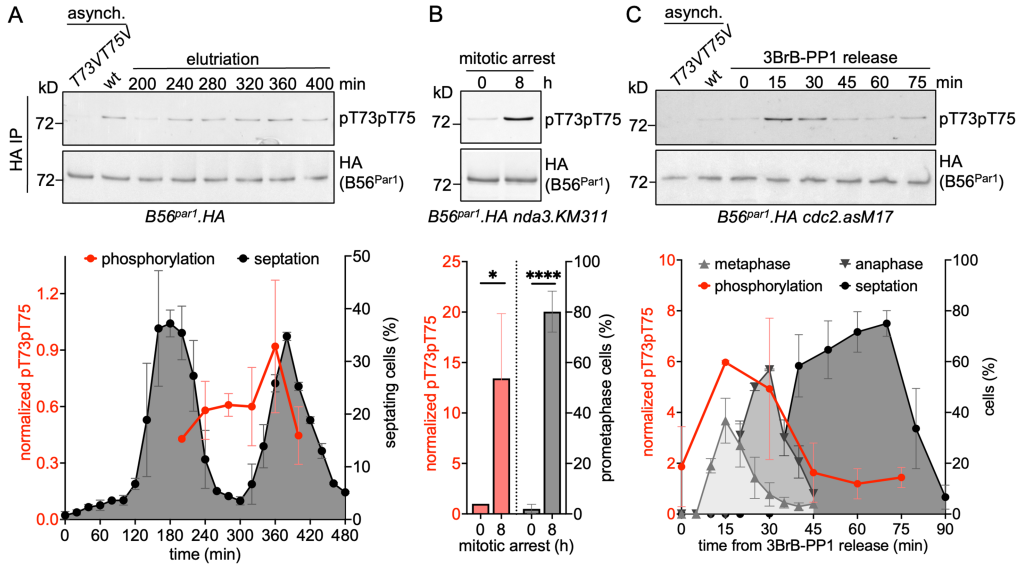

Figure 2. PP2A-B56^{Par1}.T73T75 phosphorylation rises in G2 and peaks in mitosis. (A–C) B56^{Par1}.T73T75 phosphorylation levels in cell cycle-synchronized B56^{Par1}.HA cultures. Top, representative immunoblots with samples from asynchronous cultures as controls; bottom, quantification of phosphorylation levels alongside scores of cell cycle stages (means ± s.d., $n \geq 2$). pT73pT75 levels were normalized to total levels of the B56^{Par1}.HA target protein run on a parallel Western blot as sample processing controls, and normalized values were plotted relative to asynchronous wild type, which was set to 1. (A) Centrifugal elutriation. Cell cycle progression was monitored by scores of septating cells. (B) *nda3.KM311*-mediated mitotic arrest. Arrest was monitored by the accumulation of prometaphase cells that displayed condensed chromosomes. Significance was calculated by a ratio paired *t*-test, $*p < 0.05$ (phosphorylation levels), and an unpaired *t*-test, $****p < 0.0001$ (mitotically arrested cells). (C) Mitotic progression of *cdc2.asM17* cultures upon release from 3BrB-PP1-induced G2 arrest. Cell cycle phases were monitored by scoring for metaphase, anaphase and septating cells. wt, wild type.

phosphatase assays with recombinant PP1Cα (MRC PPU Reagents and Services, University of Dundee, cat. no DU46517). PP1Cα directly dephosphorylated B56^{Par1}.T73T75, while the reaction was inhibited by the addition of the PP1 inhibitor okadaic acid (Sigma, cat. no. 495604; figure 1F). This result established that PP1 can directly target B56^{Par1}.T73T75 *in vitro*.

We have previously shown that, at mitotic exit and as part of the PP1-PP2A phosphatase relay [28], PP1^{Dis2} directly binds B56^{Par1} via G/SILK/R and K/RxVxF motifs located within the conserved common B56 core, and that mutating both motifs (*B56^{par1}.PDSN*, supplementary material, figure S1C) abolished this interaction [28]. To determine whether PP1^{Dis2}-mediated dephosphorylation of B56^{Par1}.T73T75 depends on PP1^{Dis2} docking to B56^{Par1}, we monitored the level of T73T75 phosphorylation in the *B56^{par1}.PDSN* mutant. We reasoned that if the dephosphorylation requires PP1^{Dis2} docking to B56^{Par1}, the docking site mutant would mimic the elevated T73T75 phosphorylation seen in Δ*PP1^{dis2}* (figure 1E). Interestingly, the phosphorylation of B56^{Par1}.PDSN remained at wild-type levels (figure 1G), indicating that in cells, PP1^{Dis2} does not target B56^{Par1}.T73T75 phosphorylation via docking to the G/SILK/R and K/RxVxF motifs in B56^{Par1}.

These results show that although PP1^{Dis2} can directly dephosphorylate B56^{Par1}.T73T75 *in vitro*, the dephosphorylation in cells is independent of the PP1^{Dis2} docking site on B56^{Par1}. Therefore, T73T75 is unlikely to represent a direct PP1^{Dis2} target within the PP1-PP2A mitotic phosphatase relay [28], but instead defines a novel PP1^{Dis2}-dependent mode of PP2A-B56^{Par1} regulation (figure 1H).

Both threonines T73 and T75 are flanked by prolines (figure 1C,D). Since TP sites are often targeted by CDKs to regulate cell cycle progression [49], we next asked if the phosphorylation was cell-cycle regulated.

2.3. PP2A-B56^{Par1}.T73T75 phosphorylation rises in G2 and peaks in mitosis

To monitor the phosphorylation in an unperturbed cell cycle, we followed cells as they progressed through cell division in cultures synchronized by centrifugal elutriation. *S. pombe* cells grown in standard minimal media divide after already completing S phase and are born in G2 phase of the cell cycle [50]. Centrifugal elutriation isolates these small G2 cells, which can then be followed over two subsequent cell division cycles, with the first cycle still showing stress response, while the second cycle represents an unperturbed division [51]. B56^{Par1}.T73T75 phosphorylation levels rose as septation (monitored with calcofluor (fluorescent brightener 28, Sigma, cat. no. F3543) staining) of the first cell division cycle began to cease and then peaked just before the second round of division, indicating that T73T75 phosphorylation rises in G2 and is maximal during mitosis (figure 2A).

To confirm that the B56^{Par1}.T73T75 phosphorylation increases in mitosis with a more robust cell synchronization protocol, we took advantage of the *nda3.KM311* thermosensitive β-tubulin mutant, which arrests cells in mitotic prometaphase at restrictive temperature [52,53]. B56^{Par1}.T73T75 phosphorylation was strongly upregulated in the mitotically arrested sample (figure 2B).

To further investigate the dynamics of the phosphorylation during mitotic progression, we then followed the phosphorylation kinetics as cells progressed through the different mitotic phases in adenosine triphosphate (ATP) analogue 3BrB-PP1

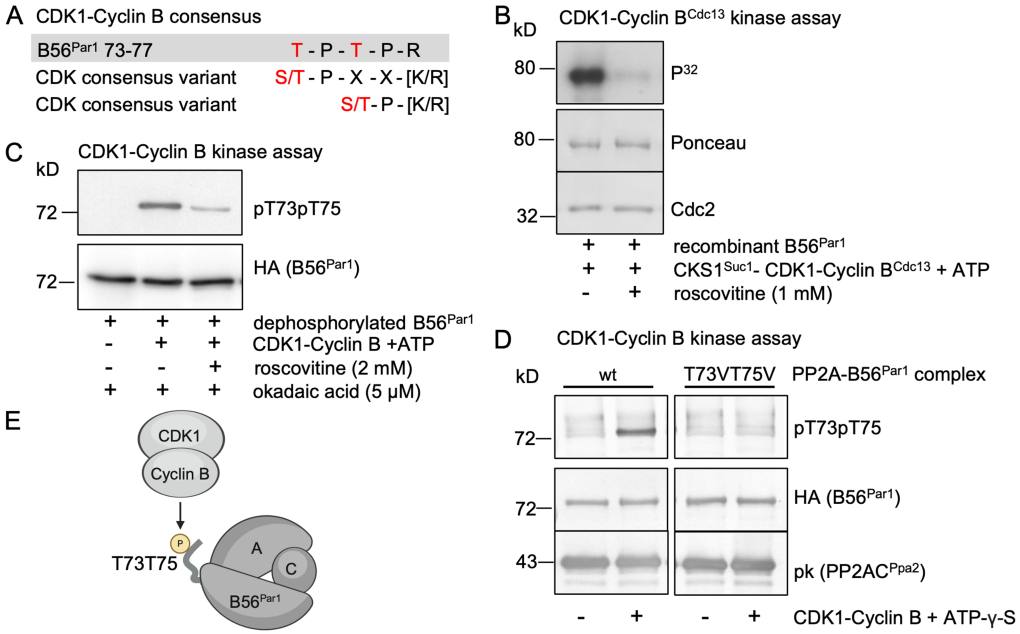

Figure 3. CDK1-Cyclin B phosphorylates PP2A-B56^{Par1}.T73T75. (A) The sequence surrounding the B56^{Par1}.T73T75 phospho-site alongside consensus variant sequences for CDK phosphorylation. (B–D) Phosphorylation of B56^{Par1} by CDK1-Cyclin B in an *in vitro* kinase assay. (B) Recombinant B56^{Par1} was phosphorylated (± CDK inhibitor roscovitine) by CDK1-Cyclin B^{Cdc13} precipitated from mitotic *S. pombe* cells by CKS1^{Suc1} affinity. Phosphorylation was detected by autoradiography. Ponceau staining and anti-Cdc2 antibodies against the fission yeast CDK1 were used as loading controls. (C) B56^{Par1}.HA was HA-immunoprecipitated from asynchronous *S. pombe* cultures under denaturing conditions, dephosphorylated by PP1 and then phosphorylated by recombinant CDK1-Cyclin B (± CDK inhibitor roscovitine) in the presence of the PP1 inhibitor okadaic acid. Phosphorylation was detected by pT73pT75 phospho-specific antibodies and B56^{Par1}.HA levels were analysed in a parallel loading on the same Western blot as sample processing controls. (D) Endogenous PP2A-B56^{Par1}.HA and PP2A-B56^{Par1}.T73VT75V.HA complexes were purified from asynchronous cultures and subjected to *thio*-phosphorylation by recombinant CDK1-Cyclin B and ATP-γ-S. Phosphorylation was detected by pT73pT75 phospho-specific antibodies, and B56^{Par1} and PP2AC^{Ppa2} levels were analysed on a parallel Western blot as sample processing controls. (E) Schematic depicting that CDK1-Cyclin B directly phosphorylates PP2A-B56^{Par1} at T73T75. C, catalytic subunit; A, scaffolding subunit; wt, wild type.

(custom made by Toronto Research Chemical)-synchronized *cdc2.as-M17* cultures [54]. In parallel with sampling for B56^{Par1}.T73T75 phosphorylation, we quantified the frequency of metaphase, anaphase and septating cells by staining for alpha tubulin (anti-Tat1 antibody [55], mitotic spindles), DAPI (Scientific Laboratory Supplies D9542, nuclei) and calcofluor (septa). This analysis revealed that T73T75 phosphorylation peaks in metaphase and then declines as cells complete anaphase (figure 2C).

Taken together, these results show that B56^{Par1}.T73T75 phosphorylation rises in the G2 phase of the cell cycle, peaks in mitosis and declines upon mitotic exit.

2.4. CDK1-Cyclin B phosphorylates PP2A-B56^{Par1}.T73T75

The mitotic up-regulation of the phosphorylation prompted us to ask whether it is directly mediated by the major mitotic kinase CDK1-Cyclin B. Sequences surrounding threonines 73 and 75 match a long [S/T]-P-x-x-[K/R] or short [S/T]-P-[K/R] CDK1 phosphorylation consensus sequence variants, respectively (figure 3A). To address whether CDK1-Cyclin B directly phosphorylates these residues, we first asked whether B56^{Par1} serves as a CDK1 phosphorylation substrate. CDK1-Cyclin B^{Cdc13} immunoprecipitated from mitotic *S. pombe* cells using CKS1^{Suc1} affinity directly phosphorylated recombinant B56^{Par1}.GST *in vitro*, while the phosphorylation was inhibited in the presence of the CDK inhibitor roscovitine (EMD Millipore, cat. no. 557364; figure 3B). This result demonstrates that CDK1-Cyclin B can act as a B56^{Par1} kinase.

We next asked whether CDK1 directly phosphorylated B56^{Par1} isolated from yeast. We immuno-precipitated B56^{Par1}.HA from asynchronous *S. pombe* cultures by HA affinity under denaturing conditions, and dephosphorylated the precipitate with recombinant PP1C*α*. The now dephosphorylated B56^{Par1}.HA was then used as a substrate for recombinant CDK1-Cyclin B (Invitrogen, cat. no. PV3292), in the presence of the PP1 and PP2A inhibitor okadaic acid to prevent any dephosphorylations. To determine if CDK1 phosphorylated B56^{Par1}.HA on T73T75, we monitored phosphorylation with pT73pT75 phospho-specific antibodies. CDK1-Cyclin B directly phosphorylated B56^{Par1} on T73T75 (figure 3C).

The assays shown in figure 3B,C utilized an isolated B56^{Par1} molecule as the kinase substrate. In cells, however, B56^{Par1} functions as part of the trimeric PP2A-B56^{Par1} complex. To determine whether CDK1-Cyclin B phosphorylates T73T75 of B56^{Par1} when incorporated into the PP2A complex, we purified endogenous PP2A-B56^{Par1} by sequential tandem affinity purification (TAP) tag and HA affinities [28]. The purified complex was then used as a substrate in the recombinant CDK1-Cyclin B kinase assays performed in the presence of a non-hydrolysable ATP analogue ATP-γ-S to prevent dephosphorylation. Importantly, CDK1-Cyclin B directly phosphorylated T73T75 when B56^{Par1} was purified as part of the endogenous PP2A-B56^{Par1} complex (figure 3D). Interestingly, in

an assay with hydrolysable ATP, CDK1-Cyclin B could only phosphorylate the complex in the presence of a PP2A inhibitor (nM okadaic acid), indicating that PP2A-B56^{Par1} can auto-dephosphorylate in these experimental conditions (supplementary material, figure S2) [56,57].

We conclude that B56^{Par1}.T73T75 is a target for CDK1-Cyclin B phosphorylation, and that CDK1-Cyclin B directly phosphorylates PP2A-B56^{Par1} complex on T73T75 (figure 3E).

2.5. Mimicking PP2A-B56^{Par1}.T73T75 phosphorylation boosts while disabling blocks PP2A-B56^{Par1} complex activity

Phosphorylations of PP2A subunits have been shown to impact PP2A complexes function, namely activity or integrity [35,58–67]. We therefore examined the effect of the T73T75 phosphorylation on the PP2A-B56^{Par1} heterotrimer.

Since PP2A-B56 can auto-dephosphorylate (supplementary material, figure S2) [56,57], we addressed the impact of T73T75 phosphorylation on PP2A-B56^{Par1} using phospho-mimetic (T73DT75D) and non-phosphorylatable (T73VT75V) variants, which are refractory to dephosphorylation at these sites.

We first asked if mimicking or disabling T73T75 phosphorylation affected the PP2A-B56^{Par1} complexes integrity. PP2A heterotrimer assembly is a stepwise process, where the scaffold (A) subunit and the regulatory (B) subunit form a dimer, which then binds the catalytic (C) subunit to form the final heterotrimer [68]. To address complex integrity, we therefore monitored the capacity of the regulatory subunit (B56^{Par1}) to co-precipitate with the major PP2A catalytic subunit (PP2AC^{Ppa2}). Both B56^{Par1} phospho-mimicking (T73DT75D) and non-phosphorylatable (T73VT75V) mutants remained in complex with the catalytic subunit in both asynchronous and analogue-synchronized cultures as cells progressed through the different stages of mitosis (supplementary material, figure S3A,B), confirming that PP2A-B56^{Par1} complex integrity is not compromised by the T73XT75X mutation.

In vertebrates, phosphorylations of the N-terminal B56 arm at distinct serine residues by checkpoint, PKA or PKC kinases were shown to either activate [61,63,65] or inhibit [67] PP2A-B56 holoenzymes. We, therefore, asked if the CDK1-Cyclin B-mediated phosphorylation of the threonine-proline sites identified in our study modulates PP2A-B56^{Par1} phosphatase activity. We addressed the question by measuring the activities of phospho-blocking or phospho-mimetic PP2A-B56^{Par1}.T73XT75X mutant complexes. To this end, we purified the major endogenous PP2A-B56^{Par1} complexes (A^{Paa1}-B56^{Par1}-C^{Ppa2} [40]) by sequential TAP tag and HA affinities from *S. pombe* cells [28] (supplementary material, figure S4A and data 2). To measure the purified complexes activities, we adopted a phosphatase assay developed for human PP2A-B56 [24,69]. The substrate in this assay is an engineered Cdc20 fragment fused to a PP2A-B56 docking site motif LDTIQEEE (LxxIxE) and phosphorylated on threonine-proline sites by Cdk1-Cyclin B. The assay was optimized to measure substrate dephosphorylation over a period of up to two hours (supplementary material, figure S4B,C).

T73T75 phosphorylation is maximal in mitosis (figure 2A–C), which prompted us to determine the impact of the T73XT75X mutations on the activity of PP2A-B56^{Par1} complexes purified from mitotic cells. We arrested cells expressing endogenous T73XT75X complexes variants in mitosis by *nda3.KM311*-mediated arrest (supplementary material, figure S5A) and purified the PP2A-B56^{Par1} complexes by sequential TAP tag–HA tag affinities. We then measured the purified mitotic complexes activity towards phosphorylated Cdc20-LxxIxE. The phospho-mimetic variant of the complex (T73DT75D) was able to dephosphorylate the substrate with faster kinetics compared to wild type, while the non-phosphorylatable variant (T73VT75V) was less effective (figure 4A–C). The activity was blocked by a PP2A inhibitor (supplementary material, figure S5B,C). A similar trend in activities of the T73DT75D and T73VT75V variants was observed with purifications from asynchronous cultures (supplementary material, figure S6A–C).

These results indicate that phosphorylation of B56^{Par1}.T73T75 increases the PP2A-B56^{Par1} complex activity, while disabling the phosphorylation blocks activity.

2.6. T73T75 phosphorylation represents a control distinct from PP2A-B56^{Par1} role in mitotic exit

As B56^{Par1}.T73T75 phosphorylation increases at G2/M transition and declines upon mitotic exit (figure 2A–C), we next examined the requirement of the B56^{Par1}.T73T75 phosphorylation for mitotic progression. To this end, we generated endogenous un-tagged *B56^{par1}* non-phosphorylatable (*T73VT75V*) and phospho-mimetic (*T73DT75D*) mutants and assessed their phenotypes.

PP2A-B56 has been shown to regulate events at metaphase/anaphase transition in both fission yeast [28,39,43,70] and higher eukaryotes [29,38,71–75]. In fission yeast, B56^{Par1} is also required for cytokinesis [76]. To ask if the phosphorylation impacts mitotic exit, we monitored the variants' progression through mitosis and cytokinesis in analogue-synchronized cultures. Both *T73DT75D* and *T73VT75V* mutants progressed normally through the different mitotic phases and septation (figure 5A), indicating that the phosphorylation was not required for mitotic exit and cytokinesis.

Although not a key player, PP2A-B56^{Par1} has been shown to function in SAC silencing [43]. Mutations in genes required for chromosome segregation, such as kinetochore-related or SAC-related genes, sensitize *S. pombe* cells to a microtubule-destabilizing drug, thiabendazole (TBZ, Toronto Research Chemicals, cat. no. T344150 [78,79]). Δ*B56^{par1}* cells show TBZ sensitivity [70]. To test the role of the T73T75 phosphorylation in SAC control, we assessed the phospho-mutants' growth in the presence of TBZ. Increasing concentrations of TBZ had no impact on the growth of *B56^{par1}.T73XT75X* (figure 5B), suggesting a normal SAC function. In addition to TBZ sensitivity, Δ*B56^{par1}* cells experience chromosome segregation errors [28]. We therefore addressed the chromosome segregation fidelity of *T73XT75X* mutants in an assay that measures the stability of an artificial mini-chromosome Ch16 [80]. Ch16 stability was not affected by either of the *B56^{par1}.T73XT75X* phospho-mutations (figure 5C). These results demonstrate that under our experimental conditions, T73T75 phosphorylation has no impact on SAC control or chromosome segregation fidelity.

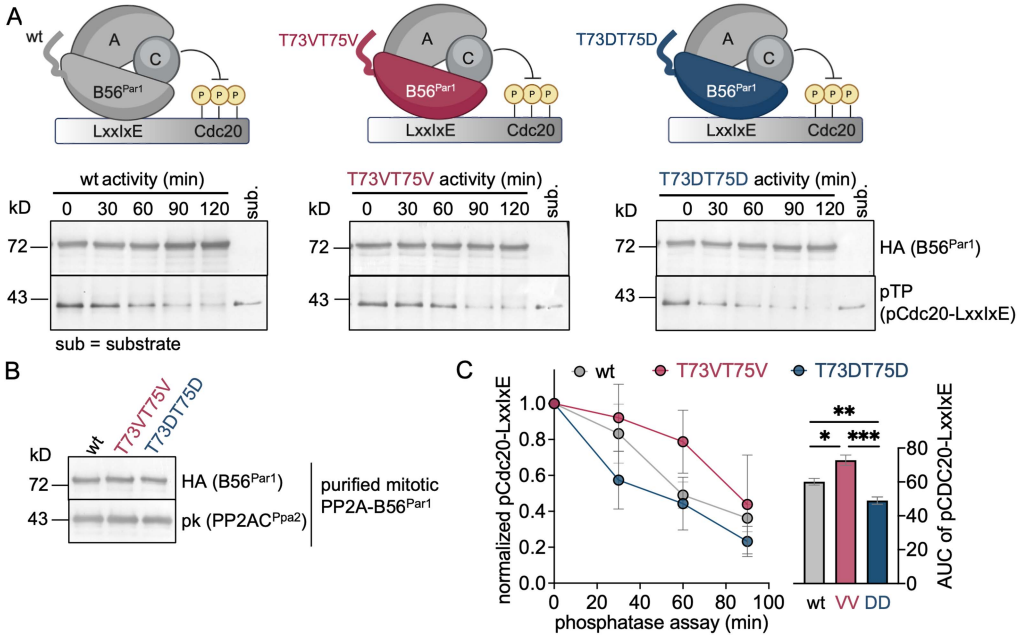

Figure 4. Mimicking PP2A-B56^{Par1}.T73T75 phosphorylation boosts while disabling blocks PP2A-B56^{Par1} complex activity. (A–C) Activity assay of purified endogenous PP2A-B56^{Par1}.T73XT75X complexes variants. (A) Activity was measured *in vitro* by monitoring the rate of dephosphorylation of a Cdc20 substrate harbouring the PP2A-B56 LxxIxE docking motif [24]. (B) Equal amounts of purified mitotic PP2A-B56^{Par1} complexes variants were mixed with a phosphorylated Cdc20-LxxIxE substrate, and dephosphorylation was monitored for 120 minutes with aliquots withdrawn in every 30 minutes. (C) Quantification of activity measured in A by level of substrate dephosphorylation (means ± s.d., $n = 4$). pCdc20-LxxIxE levels were normalized against loading control (B56^{Par1}.HA), and normalized values were plotted relative to time point 0 minute, which was set to 1. Area under the curve (AUC) significance was calculated by unpaired *t*-test, $*p < 0.05$, $**p < 0.01$, $***p < 0.001$. T73VT75V, B56^{Par1}.T73VT75V.HA complex; T73DT75D, B56^{Par1}.T73DT75D.HA complex; wt, wild-type complex; sub., substrate only.

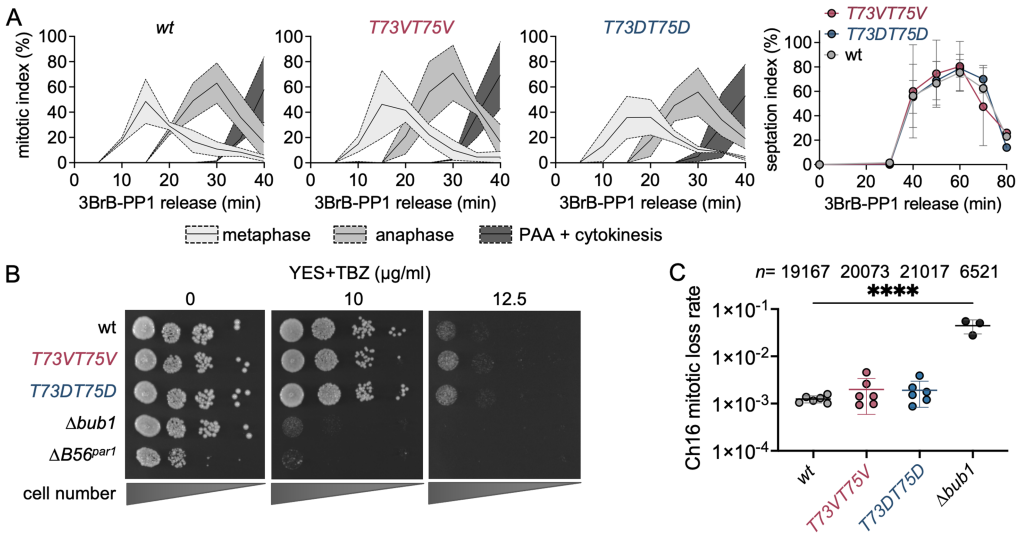

Figure 5. PP2A-B56^{Par1}.T73T75 phosphorylation is not required for mitotic exit. (A) Mitotic index (left) and septation index (right) of *cdc2.as-M17 B56^{par1}.T73XT75X* cultures upon release from 3BrB-PP1-induced G2 arrest (means ± s.d., $n = 2$). (B) Spot test of serial dilutions of asynchronous yeast cultures assessing TBZ sensitivity. The Δ*bub1* strain lacking the essential SAC component Bub1 [77] was used as a SAC-deficient control. (C) Ch16 mitotic loss assay. The Δ*bub1* strain was used as a chromosome segregation fidelity-deficient control. Significance was calculated by a one-way ANOVA followed by Dunnett's multiple comparisons test, $****p < 0.0001$.

Taken together, these results indicate that T73T75 phosphorylation is obsolete once cells are in mitosis and represents a control that is distinct from known PP2A-B56^{Par1} functions in mitotic exit and cytokinesis.

2.7. Blocking PP2A-B56^{Par1}.T73T75 phosphorylation leads to premature division at a smaller cell size

We next investigated the role of T73T75 phosphorylation in G2/M transition. Δ*B56^{par1}* cells divide at a wide distribution of sizes, at an average cell size that is approximately 1 µm smaller than wild type, which represents a reduction of approximately 9% (figure 6A,B) [28,70]. This cell size phenotype implies that the activity of PP2A-B56^{Par1} is required for cell size

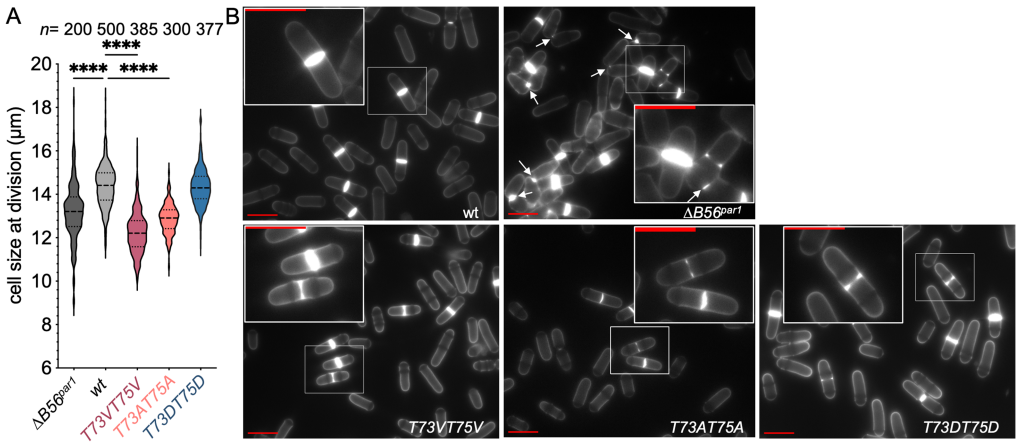

Figure 6. Blocking PP2A-B56^{Par1}.T73T75 phosphorylation induces premature division at a reduced cell size. (A,B) Cell size at division of asynchronous unperturbed cultures of endogenous B56^{Par1}.T73XT75X mutants. (A) Quantification of cell division sizes. Δ*B56^{par1}* and phospho-blocking *B56^{par1}.T73VT75V* and *B56^{par1}.T73AT75A* divide at a reduced cell size. Significance was calculated by Kruskal-Wallis's test followed by Dunn's multiple comparisons test. $^{**}p < 0.01$, $^{****}p < 0.0001$. (B) Representative images with inset magnifications of calcofluor-stained cultures. Arrowheads mark septation defects present in Δ*B56^{par1}*. Scale bar, 10 µm.

control at division. Additionally, Δ*B56^{par1}* cells exhibit morphological and septation defects (arrowheads in figure 6B), consistent with PP2A-B56^{Par1} role in cell polarity and cytokinesis [40,70,76,81,82]. Intriguingly, cells expressing the non-phosphorylatable *B56^{par1}.T73VT75V* mutant divided at an average cell length approximately 2 µm shorter than wild type, corresponding to a 15% reduction in cell length (figure 6A,B). To corroborate this finding, we generated an independent non-phosphorylatable variant, *B56^{par1}.T73AT75A*, and observed a similar small-size phenotype. These results show that blocking T73T75 phosphorylation leads to division at a reduced cell size. In line with that, phospho-mimetic *B56^{par1}.T73DT75D* maintained wild-type length at division (figure 6A,B). Neither *T73XT75X* mutant displayed morphological or septation defects seen in Δ*B56^{par1}*.

In media with glucose and a rich nitrogen source, such as EMM2 used in our study, *S. pombe* cells only grow in the G2 phase of the cell cycle (owing to a cryptic G1 cell size checkpoint) and arrest growth as they commit to mitosis with a defined cell size. Cell size at division is therefore a function of mitotic entry timing [50,83,84].

We conclude that B56^{Par1}.T73T75 phosphorylation is required to maintain cell size control at mitotic entry in unperturbed cycles. Disabling T73T75 phosphorylation leads to premature entry into mitosis at an approximately 2 µm smaller cell size, representing a 15% reduction in cell length.

3. Discussion

We initiated the present study by searching for PP1^{Dis2} target sites on B56^{Par1}, which led to the identification of proline-directed regulatory sites T73T75 in the N-terminal arm of B56^{Par1}. Previously, we demonstrated that PP1^{Dis2} directly regulates PP2A-B56^{Par1} during mitotic exit through docking to G/SILK/R and K/RxVxF motifs on B56^{Par1} [28]. By contrast, the regulatory mechanism described here is independent of this docking interaction (figure 1G), raising the possibility that PP1^{Dis2} interacts with B56^{Par1} through an additional alternative mechanism or exerts its effect indirectly. The latter is supported by observations that both PP1 and PP2A-B56 dock to regulatory or intermediate targets that subsequently recruit them to their substrates [19,85].

Analysis of endogenous T73T75 phospho-mutants revealed an outstanding cell size phenotype. Blocking B56^{Par1}.T73T75 phosphorylation reduced cell length at division in unperturbed cycles from 14 to 12 µm (figure 6A,B), dramatically altering the surface area-to-volume ratio. In *S. pombe*, which in standard media grows in the G2 phase of the cell cycle, such cell length reduction demonstrated that the phospho-blocking mutant prematurely unlocked mitotic CDK activity [11,12,50,83,84].

The B56^{Par1}.T73T75 phosphorylation is directly mediated by CDK1-Cyclin B (figure 3A–E), and phospho-mimicking mutation increases PP2A-B56^{Par1} phosphatase activity while non-phosphorylatable blocks activity (figure 4A–C; supplementary material, figure S6A–C). This is consistent with evidence from experiments with vertebrate PP2A-B56δ, where phosphorylation of the long disordered B56δ N-terminal arm by PKA or checkpoint kinases increases the holoenzyme phosphatase activity [61,63]. Cryo-electron microscopy models suggest that the activation is owing to conformational changes that enable substrate access to the catalytic site [65]. We hypothesize that by phosphorylating T73T75, the rising CDK1-Cyclin B activity concurrently activates a pool of the counteracting PP2A-B56^{Par1} phosphatase, limiting net accumulation of substrates phosphorylations. This CDK1-Cyclin B and PP2A-B56^{Par1} interplay is potentially local. The active phospho-mimetic *PP2A-B56^{par1}.T73DT75D* mutant maintains cell size threshold at mitotic entry (figure 6A,B). This suggests that in wild-type unperturbed divisions, the local PP2A-B56^{Par1} responsible for modulating cell size is maximally phosphorylated on T73T75 and active at the time of G2/M transition. Blocking T73T75 phosphorylation reduces PP2A-B56^{Par1} activity, potentially leading to increased substrates phosphorylations, which results in an accelerated mitotic onset and division at an approximately 2 µm smaller cell size, corresponding to 15% reduction in cell length (figure 7A–C). A similar concept where phosphatase activity rises concurrently with a counteracting kinase during G2 has been proposed for PP2A-B55 in *Xenopus* [37]. Our model works with the premise that the opposing PP1^{Dis2} activity is kept low at mitotic

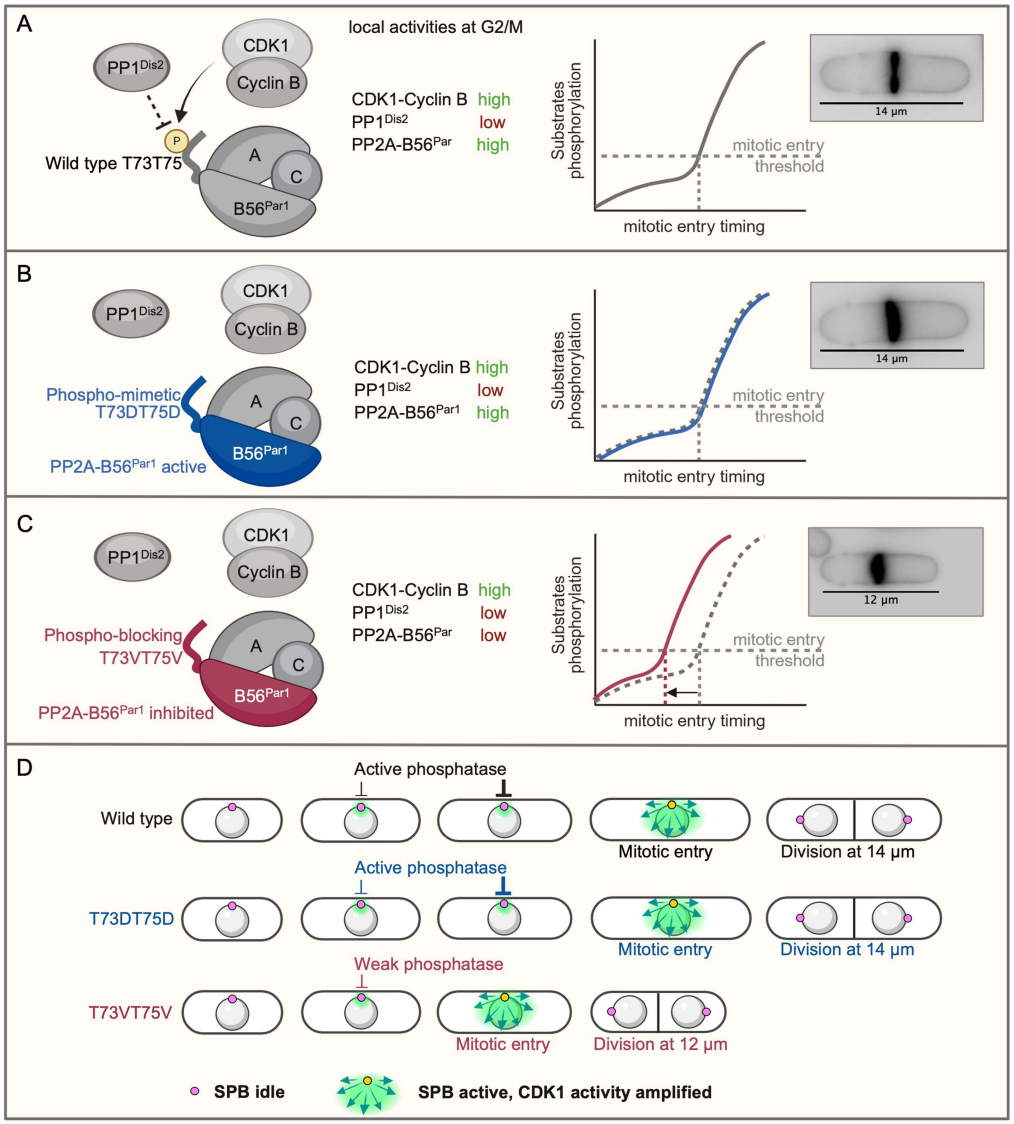

Figure 7. Model of PP2A-B56^{Par1}.T73T75 phosphorylation-mediated control of mitotic entry. (A) CDK1-Cyclin B phosphorylates B56^{Par1} on T73T75, positively regulating a local pool of the PP2A-B56^{Par1} phosphatase. At the G2/M transition, increasing CDK1-Cyclin B activity and declining PP1^{Dis2} activity [8,28,48,86] favour T73T75 phosphorylation. The locally phosphorylated PP2A-B56^{Par1} counterbalances CDK1-Cyclin B to maintain an optimal level of substrates phosphorylation and ensure a timely mitotic entry. (B) The T73DT75D phospho-mimetic mutation mimics the activity of the locally phosphorylated PP2A-B56^{Par1} pool, and cells commit to division at a wild-type threshold. (C) Disabling B56^{Par1} phosphorylation (*B56^{Par1}.T73VT75V*) results in a reduction of PP2A-B56^{Par1} activity, potentially leading to increased substrates phosphorylation. The phosphorylation threshold for mitotic entry is reached earlier and results in an advanced mitotic onset and division at an approximately 2 µm smaller cell size. Insets show representative images of dividing cells. (D) Active PP2A-B56^{Par1} (wild type or T73DT75D mutant) restricts the activity of CKD1-Cyclin B feedback loop at SPB, preventing signal amplification. The weak T73VT75V phospho-blocking mutant fails to maintain the block and prematurely unlocks the CKD1-Cyclin B feedback loop amplification, triggering advanced mitosis and division at a 2 µm smaller cell size, corresponding to a 15% reduction in cell length.

entry. This is supported by evidence from fission yeast, where commitment to mitosis is marked by CDK1-Cyclin B and NIMA^{Fin1} kinases-mediated eviction of a PP1^{Dis2} pool from the SPB [8,42]. In addition, CDK-dependent phosphorylation of a conserved C-terminal threonine negatively regulates PP1 mitotic activity [28,48,86]. Together, these mechanisms support a decrease in local PP1^{Dis2} activity at mitotic entry, thereby enabling the local net increase of PP2A-B56^{Par1}.T73T75 phosphorylation and activity.

The approximately 2 µm cell size reduction of the phospho-blocking mutant demonstrates that blocking the T73T75 phosphorylation prematurely unlocks the amplification of the CDK1/Cdc25/Wee1 feedback loop, which drives mitotic onset [11,12,50,83,84] (figure 7D). Mitosis is triggered when the CDK/Cdc25/Wee1 feedback loop signalling at the SPB overcomes inhibitory signals from counteracting phosphatases and from Wee1 signalling emanating from the cell equator [11,87,88]. Curiously, B56^{Par1} is found both on the SPB and in equatorial cortical nodes [76,89]. The premature mitosis of the lower-activity phospho-blocking *B56^{par1}.T73VT75V* mutant could result from activation of Cdc25, inhibition of Wee1 or a combination of the two. Interestingly, in *Xenopus* and human cells, PP2A-B56 has been shown to directly dephosphorylate and inactivate Cdc25, as part of the DNA-responsive checkpoint signalling in interphase [61] and at mitotic exit [90]. In fission yeast, CDK-mediated phosphorylations of Cdc25, including phosphorylations of T104 and T379, were identified as PP2A-B56 targets in a phosphoproteomic screen upon acute PP2A-B56 depletion in mitosis [15]. Additionally, the Nurse lab screen identified regulatory phosphorylation sites of the

Cdc25 phosphatase $CDC14^{Flp1}$, including inhibitory T453 phosphorylation, as PP2A-B56 substrates [15,91,92]. It remains to be determined whether PP2A-B56 prevents premature mitotic entry by inhibiting Cdc25, either directly by dephosphorylation of CDK sites or indirectly through dephosphorylation and activation of $CDC14^{Flp1}$, or through a combination of both mechanisms.

The fission yeast SPB, like the human centrosome, integrates signals from mitotic regulators [11,93–95]. Other CDK-opposed phosphatases have been shown to regulate SPB activation and modulate Cdc25 or Wee1 signalling. $PP1^{Dis2}$ recruitment to SPB governs the timing of the SPB activation in G2 [8,42]. $CDC14^{Flp1}$ eviction from the SPB at mitotic commitment reduces the local threshold for CDK1-Cyclin B activation on the SPB [91,93]. PP2A-$B55^{Pab1}$ maintains low CDK1 activity by dephosphorylating Cdc25 and Wee1, which inhibit and activate the respective CDK1 regulators [41,96], while Wee1 localized to cortical 'nodes' that form a band around the cell equator blocks propagation of feedback loop signalling from the SPB [88]. The above discussion, together with our observation that PP2A-$B56^{Par1}$ mutant cells divide at a 2 µm smaller cell size, supports a tentative model in which the SPB integrates diverse CDK-opposed phosphatase signalling prior to mitosis. We propose that phosphatase inputs converging at the SPB are integrated into a coherent signal that is amplified throughout the cell to regulate mitotic entry. Although speculative, this model provides a useful framework for future experimental investigations.

Phosphatases are notoriously difficult to study because their disruption often leads to pleiotropic defects. Here, we have identified a regulatory site on PP2A-$B56^{Par1}$ that specifically controls the timing of mitotic entry. Furthermore, to our knowledge, this study is the first to demonstrate in any organism that PP2A-B56 regulation controls mitotic entry timing during unperturbed cycles. The threonine-proline module is conserved in analogous regions of B56 orthologues, including humans (figure 1D). Given the broad conservation of cell cycle control by CDK-opposed phosphatases from *S. pombe* to higher eukaryotes, it is likely that similar regulatory mechanisms operate in human cells.

4. Materials and methods

4.1. Yeast cell culture

S. pombe strains used for this study are listed in table S1 in the supplementary material. Reagents and resources used in this study are listed in table 1. For standard growth and cell cycle synchronization assays by elutriation or the ATP analogue 3BrB-PP1, cells from –70°C glycerol stocks were streaked on Yeast extract with supplements (YES) media (0.5% yeast extract, 3% D-glucose, 250 mg l^{-1} adenine (Sigma A9126), histidine (Sigma H5659), leucine (Sigma L8000), uridine (Sigma U3750) and lysine (Sigma L9037)), and then grown in liquid Edinburgh minimal media 2 (EMM2, supplementary material, table S2) without supplements (unless otherwise specified) at 25°C in the log phase for 48 hours until the density of 2×10^6 cells ml^{-1}. For cell size measurement experiments, cells were grown in EMM2 without supplements at 32°C in the log phase for 48 hours until the density of 2×10^6 cells ml^{-1}.

Centrifugal elutriation was performed as described [51]. For ATP-analogue synchronizations of mitotic entry, *cdc2.as-M17* cultures were arrested in G2 for 4 hours 15 minutes by 2 µM ATP-analogue 3Br-BPP1 and then filtered into a fresh media to release from inhibition [54]. For *nda3.KM311*–mediated arrest, cultures were grown in YES at permissive temperature in the log phase for 48 hours and the arrest was performed in YES for 8 hours at the restrictive temperature of 20°C [53].

For large-scale affinity purifications, cells were inoculated in YES medium overnight and then diluted in 2× concentrated YES+AA and grown for 48 hours up to the density of 1×10^8 cells ml^{-1}.

4.2. Large-scale affinity purification for quantitative mass spectrometry

In total, 2×10^{11} cells per sample were processed according to a standard protocol [45]. Briefly, cells were cryo-milled under liquid nitrogen in a SPEX Sample Prep 6875D freezer mill (Wolflabs, eight cycles 2-2-2 with an impact rate of 14). Solubilization was achieved by the addition of 6% SDS and immunoprecipitation (IP) was performed under denaturing conditions [45] with HA-affinity (Pierce anti-HA magnetic beads, Thermo Scientific, cat. no. 88837) in IP buffer (50 mM Hepes pH 7.5, 1 mM ethylenediaminetetraacetic acid (EDTA), 100 mM NaCl, 20 mM Na-β-glycerophosphate, 2 mM Na_3VO_4, 50 mM sodium fluoride (NaF), 0.1% NP40, 1 mM phenylmethylsulfonyl fluoride (PMSF), cOmplete™ EDTA-free Protease Inhibitor Cocktail, Merck 05056489001) with 1mM dithiothreitol (DTT) for 1 hour at 4°C. HA-precipitates were resolved in a 4%–12% 2-[bis(2-hydroxyethyl)amino]-2-(hydroxymethyl)propane-1,3-diol (Bis-Tris) gel (NuPage NP0322BOX) and stained with Coomassie Brilliant Blue G-Colloidal concentrate (Merck B2025).

4.3. Mass spectrometry

Protein bands were excised from the gel destained with three 10 minute washes in 1 ml high-performance liquid chromatography (HPLC) grade water with 40% acetonitrile and 200 mM ammonium bicarbonate. Samples were then cleaned with a 10-minute wash with 1ml HPLC-grade water followed by dehydration with 1 ml of acetonitrile. This cycle of hydration-dehydration was performed a total of three times followed by vacuum centrifugation. Protein bands were digested with 20 ng sequencing-grade trypsin in 100 µl of 40 mM ammonium bicarbonate with 9% (v/v) acetonitrile at 37°C for 18 hours. The peptides were separated using an RSLCnano ultra-high performance liquid chromatography (UPLC) system (Thermo Scientific) using a Thermo pepmap C18 EasySpray column (75 µm inner diameter, 2 µm and 50 cm) with a gradient of 1–25% (v/v) of acetonitrile with 0.1% formic

Table 1. Reagents and resources used in this study.

reagent/resource	reference or source	identifier or catalogue number
experimental models		
S. pombe strains	this study and others	supplementary table S1
E. coli BL21 CodonPlus	lab stock	
E. coli BL21(DE3)-RIL	gift from Lowe lab	
recombinant DNA		
pETDuet-1 *His.B56^{par1}*	this study	N/A
TOPO *pk.PP2AC^{ppa2}:hpHMX6*	this study	N/A
TOPO *B56^{par1}*	Grallert *et al.* [28]	N/A
pRK753 *MBP.His.TEV*	gift from Lowe lab	N/A
pET41 *Cdc20$^{49-78}$.LDTIQEE*	this study	N/A
antibodies		
rabbit anti-phospho-B56^{Par1}.T73T75	Eurogentec	custom generated
goat anti-rabbit IgG AP	Sigma	A3687
goat anti-mouse IgG AP	Sigma	A3688
mouse anti-V5-Tag clone SV5-Pk1	BioRad	MCA1360
mouse anti-Cdc2	Abcam	Ab5467
mouse anti-HA clone 12CA5 tissue culture supernatant	lab stock	N/A
goat anti-mouse IgG HRP	Cell Signaling	7076P2
mouse anti-phospho-threonine-proline	Cell Signaling	9391S
mouse anti-Tat1	Gull lab [55]	N/A
goat anti-mouse IgG FITC	Sigma	F0257
oligonucleotides and other sequence-based reagents		
B56^{par1} tagging primer forward		AACTTAAATCTCAAAACCCTACTACTGTGCACTCTACTACTGAGAGACTAAAAAAACTTTCACTTGACTACACCAATGGTCGGATCCCCGGGTTAATTAA
B56^{par1} tagging primer reverse		TAACTGAAAATGATATAGTATGTAAAATGTAAAAGAGGGAATATTAGAGAGACTAAGTACAATATATGGATCATTATTAAAAGAATTCGAGCTCGTTTAAAC
TOPO *PP2AC^{ppa2}* forward	ACTATGTACGCTTCTTCTCG	
TOPO *PP2AC^{ppa2}* reverse	CCTTGAGTACTCTTCTTGCCTTCAA	
PP2AC^{ppa2} tagging primer 1	TAATTATGGAATTTTGTATATAGTAAAAAG	

(*Continued.*)

Table 1. (*Continued.*)

reagent/resource	reference or source	identifier or catalogue number
PP2AC^{ppa2} tagging primer 2	ATATACAAAATTCCATAATTAATGGGTATTCCTAACCCTTTG	
PP2AC^{ppa2} tagging primer 3	CCTTAGTGTTCACTTACCTTATCGCATAACATTTCAAC	
PP2AC^{ppa2} tagging primer 4	GTAAGTGAACACTAAGGAGAGTATATATG	
pk.PP2AC^{ppa2} *hpHMX6* primer 1	AATTCTCTAATGAGTGATCAATC	
pk.PP2AC^{ppa2} *hpHMX6* primer 2	CCTTCGAGCTATTACCGG	
pk.PP2AC^{ppa2} *hpHMX6* primer 3	AAGTCTTTTTACAATTCGATCCTGCCCCACGAGAAGGCGAACCGGTAATAGCTCGAAGGACACCAGACTACTTCCTTTAATGATAGCGGATCCCCGGGTT	
pk.PP2AC^{ppa2} *hpHMX6* primer 4	TAATCTTGAGTATTAACTCAAAAATCAGAAAGGTGGATAAATTTTTTGAAACAATCACAATCGATTGATCACTCATTAGAGAATTCGAGCTCGTTTAAAC	
B56^{par1}*.T73VT75V* mutagenesis primer forward:	AAGTACCTATTGATACCGTACCAGTACCTAGAGATGAGATCTT	
B56^{par1}*.T73VT75V* mutagenesis primer reverse:	AAGATCTCATCTCTAGGTACTGGTACGGTATCAATAGGTACTT	
B56^{par1}*.T73DT75D* mutagenesis primer forward:	AAGTACCTATTGATACCGATCCAGATCCTAGAGATGAGATCTT	
B56^{par1}*.T73DT75D* mutagenesis primer reverse:	AAGATCTCATCTCTAGGATCTGGATCGGTATCAATAGGTACTT	
B56^{par1}*.T73AT75A* mutagenesis primer forward:	AAGTACCTATTGATACCGCACCAGCACCTAGAGATGAGATCTT	
B56^{par1}*.T73AT75A* mutagenesis primer reverse:	AAGATCTCATCTCTAGGTGCTGGTGCGGTATCAATAGGTACTT	
chemicals, enzymes and other reagents		
yeast extract	Appleton Woods	212750
D-glucose	VWR	101176K
adenine	Sigma	A9126
histidine	Sigma	H5659
leucine	Sigma	L8000
uridine	Sigma	U3750
lysine	Sigma	L9037
EMM2	Nurse, 1975	for composition, see Supplementary table S2
L-glutamic acid	Sigma	G5889
3BrB-PP1	Toronto Research Chemicals	custom made
PP1Cα	University of Dundee	DU46517
ATP-γ-P^{32}	Hartmann Analytics	SCP-401
ATP-γ-S	Abcam	AB138911
Taq polymerase	NEB	M0273S
PfU Ultra HF polymerase	Agilent	600382

(*Continued.*)

Table 1. (*Continued.*)

reagent/resource	reference or source	identifier or catalogue number
dNTP mix 100 mM	Bioline	BIO-39029
thiabendazole	Toronto Research Chemicals	T344150
CDK1-Cyclin B active	Invitrogen	PV3292
Pierce anti-HA magnetic beads	Thermo Scientific	88837
cOmplete™ EDTA-free Protease Inhibitor Cocktail	Merck	05056489001
4-12% Bis-Tris gel	NuPage	NP0322BOX
Coomassie Brilliant Blue G-Colloidal concentrate	Merck	B2025
DAPI	scientific laboratory supplies	D9542
NBT Biochemica	PanReac Applichem	A1243
BCIP	Thermo Scientific	J64451.03
5-FOA	Sigma	F5013
Protran 0.45 µm nitrocellulose membrane	Amersham	010600002
Pierce NHS-activated magnetic beads $CKS1^{Suc1}$	Singh *et al.* [54]	N/A
Roscovitine	EMD Milipore	557364
LDS sample buffer	NuPage	2020067
trypsin sequencing grade	Sigma	11 047 841 001
Calcofluor Fluorescent Brightener 28	Sigma	F3543
protein marker	NEB	P7712
protein marker	NEB	P7719
okadaic acid	Sigma	495604
HisPurTm Ni-NTA Superflow agarose	Thermo Scientific	25216
IgG sepharose 6 fast flow	Cytiva	17096901
Pierce A/G magnetic beads anti-HA clone 12CA5	this study	N/A
HA peptide	Thermo Scientific	26184
software		
GraphPad Prism 10	https://www.graphpad.com	
Scaffold 5	https://www.proteomesoftware.com	
Scaffold PTM	https://www.proteomesoftware.com	
FiJi	https://imagej.net	
SnapGene 8.2.1	https://www.snapgene.com	

(*Continued.*)

Table 1. (*Continued.*)

reagent/resource	reference or source	identifier or catalogue number
BioRender	https://www.biorender.com	
Mascot Distiller	https://www.matrixscience.com/distiller.html	
Mascot	https://www.matrixscience.com	
Progenesis LCMS	https://www.nonlinear.com/progenesis/	
other		
Econo-Pac Chromatography columns	BioRad	
SPEX Sample Prep 6875D freezer mill	WolfLabs	
RSLC nano UPLC system	Thermo Scientific	
Orbitrap Fusion Mass Spectrometer	Thermo Fisher Scientific	
Multi-beads shocker	Yasui Kikai	
ZEISS Axio Imager.M2 microscope	Zeiss	
ZEISS Axiocam 705 mono camera	Zeiss	
Puregene Yeast/Bact. kit	Qiagen	1042607

acid over 30 minutes at a flow rate of 200 nl min^{-1}. The Orbitrap Fusion Mass Spectrometer (Thermo Fisher Scientific) was operated in data-dependent mode, where the survey scan was performed at a nominal resolution of 120 000 (at m/z 200) in the Orbitrap analyser over an m/z range of 350–1200. The instrument performed as many higher-energy collisional dissociation (HCD) second-stage mass spectrometry (MS2) scans as possible in a total cycle time of 1.1 seconds. HCD was performed at 28% normalized collision energy, and the MS2 spectra were collected in the linear ion trap. For protein identification and phospho-mapping, Mascot Generic Format datasets were generated in Mascot Distiller followed by a database search using Mascot (Matrix Science). Mascot search results were imported into Scaffold and Scaffold PTM. Label-free quantification of phosphopeptides was achieved with Progenesis LC-MS.

4.4. Genetic manipulations

To generate endogenous *B56^{par1}.T73T75* phospho-mutants, mutations encoding T73XT75X variants were introduced via site-directed mutagenesis into a Topoisomerase-based cloning (TOPO) vector harbouring B56^{Par1} open reading frame (ORF) flanked by 100 bp 5′ and 3′ untranslated regions (UTRs) [28]. The clones were transformed into *S. pombe ΔB56^{par1}* host according to standard procedures [97], selected by 5-fluoroorotic acid (5-FOA, Sigma F5013) resistance and mutation confirmed by DNA sequencing. HA-tagging of endogenous *B56^{par1}* was performed as previously described [98].

To generate *pk.PP2AC^{ppa2}*, the *PP2AC^{ppa2}* ORF flanked by 3′ and 5′ UTRs was amplified by PCR and inserted into a TOPO vector. N-terminal pk tag and hygromycin-resistant allele *hphMX6* were inserted into the resulting plasmid by Gibson assembly [99]. The *pk.ppa2:hpHMX6* cassette was then transformed into *S. pombe* Δ*PP2AC^{ppa2}* host according to standard procedures [97], clones selected by 5-FOA resistance and insertion confirmed by DNA sequencing.

4.5. Small-scale HA-affinity purification

In total, 2×10^8 cells (6×10^8 for *B56^{par1}.PDSN*) were harvested by centrifugation (3500 g for 2 minutes), washed in STOP buffer (50 mM NaF, 10 mM EDTA, 0.9% NaCl, 1 mM sodium azide [NaN_3]) at 4°C and pellets were stored at –70°C until processing. HA-affinity purification was performed as previously described under denaturing or native conditions [100]. Briefly, cell pellets were disrupted using a multi-bead shocker (Yasui Kikai) and IP was performed with Pierce HA beads in IP buffer + 1mM DTT for 1 h at 4°C.

4.6. PP1^{Dis2} phosphatase assay

B56^{Par1}.HA substrate was precipitated from wild-type cells by small-scale denaturing IP [100]. The HA-beads-bound precipitates were then washed in protein metallophosphatases (PMP) buffer (50 mM HEPES pH 7.5, 100 mM NaCl, 2 mM DTT, 0.01% Brij-35, 1 mM $MnCl_2$) and incubated in 10 µl PMP buffer with 1.38 µg PP1Cα without or with inhibitor (5 µM okadaic acid) for 1 h at 30°C.

4.7. Microscopy

Cell cycle progression was tracked by scoring the percentage of septating cells with calcofluor and/or monitoring chromatin condensation with 4′,6-diamidino-2-phenylindole (DAPI) according to standard procedures [101]. Mitotic phases were monitored by combined DAPI staining and anti-tubulin immunofluorescence with Tat1 tissue culture supernatant monoclonal antibody (1 : 80, a gift from Gull [55]), using established procedures [93,102]. Images were obtained using an Axio Imager.M2 microscope (Zeiss) with an α Plan-FLUAR 100 ×/1.45 oil objective (Zeiss) and Axiocam 705 mono camera (Zeiss) and processed with Fiji.

4.8. Recombinant protein expression and purification

B56^{par1} coding sequence (CDS; custom made by GeneArt, Life Technologies) was cloned into pETDuet-1 by Sac*I* and Not*I* restriction digest and ligation and His.B56^{Par1} was expressed in *Escherichia coli* BL21-CodonPlus. pRK753 plasmid harbouring *MBP.His.TEV* (Tobacco Etch Virus protease; a gift from M. Lowe) was expressed in *E. coli* BL21(DE3)-RIL. *Cdc20$^{49-78}$* fragment fused with 'superbinder' LxxIxE peptide LDTIQEE [24] was cloned by Nco*I* BamH*I* restriction digest and ligation into pET41 and Cdc20-LxxIxE.His was expressed in *E. coli* BL21-CodonPlus. Protein expression and purification were performed according to standard protocols with HisPur^{Tm} nitrilotriacetic acid (Ni-NTA) agarose (Thermo Scientific, cat. no. 25216) under native conditions.

4.9. PP2A-B56^{Par1} complex purification

PP2A-B56^{Par1} complexes harbouring the major catalytic subunit PP2AC^{Ppa2} were purified by sequential TAP tag and HA- affinities [28]. Briefly, 1×10^{11} cell pellets were cryo-milled under liquid nitrogen in a SPEX Sample Prep 6875D freezer mill (eight cycles 2-2-2 with impact rate of 14). Immunoglobulin G (IgG) affinity was performed with 0.5 ml IgG Sepharose 6 fast flow beads (Cytiva, cat. no. 17096901) in IP buffer without phosphatase inhibitors (50 mM Hepes pH 7.5, 1 mM EDTA, 100 mM NaCl, 1 mM PMSF, 0.1% NP40, cOmplete™ EDTA-free Protease Inhibitor Cocktail) at 4°C for 1 hour. Bound PP2A complexes were washed twice with IP buffer without phosphatase inhibitors and twice with TEV buffer (10 mM Tris pH 8.0, 150 mM NaCl, 0.1% NP40, 0.5 mM EDTA, 1 mM DTT, cOmplete™ EDTA-free Protease Inhibitor Cocktail) by gravity flow in Econo-Pac Chromatography columns (BioRad). Columns were then capped at both ends and incubated with 50 µg TEV protease and 500 µl TEV buffer at 25°C for 2 hours while gently shaking at 100 r.p.m. Flow-through was then collected and topped with IP buffer without phosphatase inhibitors up to 7 ml and incubated O/N at 4°C with 125 µl Pierce A/G beads (Thermo Scientific, cat. no. 88802) covalently coated with monoclonal 12CA5 HA antibody. The HA beads-bound PP2A-B56^{Par1} complexes were then washed 4× with IP buffer without phosphatase inhibitors at 4°C and either immediately used for enzymatic assays, or eluted at 30°C for 1 hour at 100 r.p.m. with 1 mg/ml HA peptide (Thermo Scientific, cat. no. 26184) in elution buffer (20 mM Tris pH 7.4, 150 mM NaCl, 1 mM $MnCl_2$, cOmplete EDTA-free Protease Inhibitor Cocktail) for protein identification by Mass Spectrometry.

4.10. PP2A-B56^{Par1} activity assay

Phosphatase assays were performed with purified PP2A-B56^{Par1} complexes as previously described [24]. Cdc20-LxxIxE fragment (150 µg) was phosphorylated with 0.7 µg recombinant CDK1-Cyclin B kinase and 100 µM ATP in 200 µl kinase assay buffer (KAB; 50 mM tris pH 7.4, 10 mM $MgCl_2$, 1 mM DTT, cOmplete EDTA-free Protease Inhibitor Cocktail) for 30 minutes at 30°C. The reaction was stopped with the addition of 1 mM roscovitine, buffer was then exchanged for phosphatase buffer (50 mM Tris pH 7.4, 150 mM NaCl, 1 mM $MnCl_2$, 1 mM DTT, 0.1% Igepal, cOmplete EDTA-free Protease Inhibitor Cocktail, 1 mM roscovitine) + 25% glycerol using ZebaSpin desalting columns and the phosphorylated Cdc20-LxxIxE fragment was stored in 20 µl aliquots at –80°C at the concentration of 0.4 µg µl^{-1}.

Purified PP2A-B56^{Par1} complexes bound to HA-beads were washed with phosphatase buffer in non-stick tubes on ice and then mixed with 1.2 µg of the phosphorylated Cdc20-LxxIxE substrate in 50 µl phosphatase buffer. Reaction was incubated on a rotator wheel for up to 120 minutes at 30°C with samples withdrawn at intervals. Reaction was stopped by the addition of lithium dodecyl sulfate (LDS) sample buffer (NuPage) + 25% ß-mercaptoethanol for 10 minutes at 70°C.

4.11. CDK1-Cyclin B kinase assay

For *S. pombe* CDK1-Cyclin B^{Cdc13} kinase assay, *cdc25.22* cultures grown at permissive temperature (25°C) in EMM2 + AA (EMM2 supplemented with 250 mg l^{-1} adenine, histidine, leucine, uridine and lysine) were arrested at G2/M transition by incubation at 37°C for 4 hours and 30 minutes and then released into permissive 25°C [103]. After 20 minutes, 2×10^8 cells were harvested by centrifugation (3500 *g*, 2 minutes) and CDK1-Cyclin B^{Cdc13} was precipitated by small-scale CKS1^{Suc1} affinity as previously

described [54,104]. Recombinant His.B56^{Par1} substrate (1.2 µg) was added to 20 µl CKS1^{Suc1} beads with immobilized CDK1-Cyclin B^{Cdc13}, and the kinase reaction was performed according to protocol [104] with ATP-γ-P^{32} for 10 minutes at 30°C without or with inhibitor (1 mM roscovitine).

Recombinant human CDK1-Cyclin B kinase assays were performed with B56^{Par1} substrates (B56^{Par1}.HA subunit or PP2A-B56^{Par1}.HA complex) isolated from *S. pombe*. B56^{Par1}.HA was HA-affinity purified under denaturing conditions from *S. pombe* asynchronous cultures, *in vitro* dephosphorylated with PP1Cα, washed twice with KAB and resuspended in 10 µl KAB + 5 µM okadaic acid. The PP2A-B56^{Par1}.HA complexes harbouring the major pk.PP2AC^{Ppa2} catalytic subunit and bound to HA-beads were washed twice with KAB and resuspended in 10 µl KAB ± 20 nM okadaic acid. 0.5 µg of active recombinant CDK1-Cyclin B kinase was mixed with the HA beads-bound B56^{Par1} or PP2A-B56^{Par1}, respectively, in the presence of 100 µM ATP or ATP-γ-S without or with inhibitor (roscovitine, 2 mM) and okadaic acid (5 µM) as indicated, and the reaction was incubated for 30 minutes at 30°C.

4.12. Western blotting

Proteins in LDS sample buffer + 25% ß-mercaptoethanol were heated for 10 minutes at 70°C, separated on a 4–12% Bis-Tris gel and transferred onto a nitrocellulose membrane. Ponceau staining was used as indicated to monitor total protein levels prior to probing with antibodies. Polyclonal antibodies raised against the dual-phosphorylated pT73pT75 were custom-generated and purified by Eurogentec. The following dilutions of antibodies were used in this study: anti-pk clone SV5-Pk1 (BioRad, cat. no. MCA1360; 1 : 500), tissue culture supernatant anti-HA clone 12CA5 (lab stock; 1 : 100), anti-Cdc2 (Abcam, cat. no. Ab5467; 1 : 2000), anti-phospho-threonine-proline (Cell Signaling, cat. no. 9391S; 1 : 2000) and anti-phospho-B56^{Par1}.T73T75 (custo made by Eurogentec; 1 : 1000). Horseradish peroxidase (HRP) or alkaline phosphatase-coupled secondary antibodies and chromogenic detection, chemiluminescence or autoradiography were used to detect the signals. In case of reprobing, the membrane was first incubated in a stripping buffer (0.2 mM glycine, 0.05% Tween, 0.7% ß-mercaptoethanol, pH 2.5) for 30 minutes at 60°C before probing with a second set of antibodies.

4.13. TBZ sensitivity assay

Cultures were grown exponentially for 48 hours in YES medium up to 1×10^6 cells ml^{-1}, and serial 10× dilutions were spotted onto YES plates containing increasing concentrations of TBZ. Colony formation was monitored for 4–6 days at 25°C.

4.14. Ch16 mitotic loss rate

Ch16 mitotic loss assays were performed as previously described [77]. Strains harbouring artificial Ch16 were grown exponentially for 48 hours in Edinburgh Minimal Medium Glutamate (EMMG) [105]) without supplements up to the density of 1×10^6 cells ml^{-1}, and aliquots of 10–100 µl were plated on EMMG plates supplemented with 5 mg ml^{-1} adenine. The frequency of Ch16 loss was scored by monitoring the frequency of half-sector red colonies after 6 days at 25°C.

Ethics. This work did not require ethical approval from a human subject or animal welfare committee.

Data accessibility. Mass spectrometry data associated with the manuscript are available in supplementary material as supplementary data 1 and supplementary data 2 [106].

Declaration of AI use. We have not used AI-assisted technologies in creating this article.

Authors' contributions. L.H.: conceptualization, data curation, formal analysis, investigation, methodology, project administration, supervision, validation, visualization, writing—original draft, writing—review and editing; Y.C.: investigation; D.S.: data curation, formal analysis; J.P.: supervision, writing—review and editing; I.H.: conceptualization, funding acquisition, methodology, project administration, supervision, writing—review and editing.

All authors gave final approval for publication and agreed to be held accountable for the work performed therein.

Conflict of interest declaration. We declare we have no competing interests.

Funding. This work was supported by Cancer Research UK (Grant nos. C5759/A20971 and C5759/A27412).

Acknowledgements. We thank Jon Pines for advice during the last year of the study, Ray O'Keefe, Steve High, Phil Woodman, Martin Lowe and Viki Allan for their warm support and laboratory space for a part of this study, Martin Lowe for the gift of *E.coli* BL21(DE3)-RIL [pRK753], Keith Gull for the gift of hybridoma cell line expressing Tat1 antibody and Jennifer Winstanley for assistance in the early stages of the project.

References

1. Nurse P. 1990 Universal control mechanism regulating onset of M-phase. *Nature* **344**, 503–508. (doi:10.1038/344503a0)
2. Stern B, Nurse P. 1996 A quantitative model for the cdc2 control of S phase and mitosis in fission yeast. *Trends Genet.* **12**, 345–350. (doi:10.1016/s0168-9525(96)80016-3)
3. Alfa CE, Ducommun B, Beach D, Hyams JS. 1990 Distinct nuclear and spindle pole body population of cyclin-cdc2 in fission yeast. *Nature* **347**, 680–682. (doi:10.1038/347680a0)
4. Decottignies A, Zarzov P, Nurse P. 2001 In vivo localisation of fission yeast cyclin-dependent kinase cdc2p and cyclin B cdc13p during mitosis and meiosis. *J. Cell Sci.* **114**, 2627–2640. (doi:10.1242/jcs.114.14.2627)
5. Basu S, Roberts EL, Jones AW, Swaffer MP, Snijders AP, Nurse P. 2020 The hydrophobic patch directs cyclin B to centrosomes to promote global CDK phosphorylation at mitosis. *Curr. Biol.* **30**, 883–892. (doi:10.1016/j.cub.2019.12.053)

6. Izumi T, Maller JL. 1995 Phosphorylation and activation of the *Xenopus* Cdc25 phosphatase in the absence of Cdc2 and Cdk2 kinase activity. *Mol. Biol. Cell* **6**, 215–226. (doi:10.1091/mbc.6.2.215)
7. Izumi T, Maller JL. 1993 Elimination of cdc2 phosphorylation sites in the cdc25 phosphatase blocks initiation of M-phase. *Mol. Biol. Cell* **4**, 1337–1350. (doi:10.1091/mbc.4.12.1337)
8. Grallert A *et al.* 2013 Removal of centrosomal PP1 by NIMA kinase unlocks the MPF feedback loop to promote mitotic commitment in *S. pombe*. *Curr. Biol.* **23**, 213–222. (doi:10.1016/j.cub.2012.12.039)
9. Grallert A, Patel A, Tallada VA, Chan KY, Bagley S, Krapp A, Simanis V, Hagan IM. 2013 Centrosomal MPF triggers the mitotic and morphogenetic switches of fission yeast. *Nat. Cell Biol.* **15**, 88–95. (doi:10.1038/ncb2633)
10. Mulvihill DP, Petersen J, Ohkura H, Glover DM, Hagan IM. 1999 Plo1 kinase recruitment to the spindle pole body and its role in cell division in *Schizosaccharomyces pombe*. *Mol. Biol. Cell* **10**, 2771–2785. (doi:10.1091/mbc.10.8.2771)
11. Hagan IM, Grallert A. 2013 Spatial control of mitotic commitment in fission yeast. *Biochem. Soc. Trans.* **41**, 1766–1771. (doi:10.1042/BST20130190)
12. Ferrell JE, Jr. 2008 Feedback regulation of opposing enzymes generates robust, all-or-none bistable responses. *Curr. Biol.* **18**, R244–245. (doi:10.1016/j.cub.2008.02.035)
13. Gould KL, Nurse P. 1989 Tyrosine phosphorylation of the fission yeast cdc2+ protein kinase regulates entry into mitosis. *Nature* **342**, 39–45. (doi:10.1038/342039a0)
14. Novak B, Tyson JJ. 1993 Numerical analysis of a comprehensive model of M-phase control in *Xenopus* oocyte extracts and intact embryos. *J. Cell Sci.* **106**, 1153–1168. (doi:10.1242/jcs.106.4.1153)
15. Zeisner TU, Auchynnikava T, Roberts EL, Nurse P. 2025 Phosphatase specificity influences phosphorylation timing of CDK substrates during the cell cycle. *Nat. Commun.* **16**, 11604. (doi:10.1038/s41467-025-66547-5)
16. Nilsson J. 2019 Protein phosphatases in the regulation of mitosis. *J. Cell Biol.* **218**, 395–409. (doi:10.1083/jcb.201809138)
17. Nasa I, Kettenbach AN. 2018 Coordination of protein kinase and phosphoprotein phosphatase activities in mitosis. *Front. Cell Dev. Biol.* **6**, 30. (doi:10.3389/fcell.2018.00030)
18. Moura M, Conde C. 2019 Phosphatases in mitosis: roles and regulation. *Biomolecules* **9**, 55. (doi:10.3390/biom9020055)
19. Bollen M, Peti W, Ragusa MJ, Beullens M. 2010 The extended PP1 toolkit: designed to create specificity. *Trends Biochem. Sci.* **35**, 450–458. (doi:10.1016/j.tibs.2010.03.002)
20. Lacroix B, Lorca T, Castro A. 2022 Structural, enzymatic and spatiotemporal regulation of PP2A-B55 phosphatase in the control of mitosis. *Front. Cell Dev. Biol.* **10**, 967909. (doi:10.3389/fcell.2022.967909)
21. Cundell MJ, Hutter LH, Nunes Bastos R, Poser E, Holder J, Mohammed S, Novak B, Barr FA. 2016 A PP2A-B55 recognition signal controls substrate dephosphorylation kinetics during mitotic exit. *J. Cell Biol.* **214**, 539–554. (doi:10.1083/jcb.201606033)
22. Hoermann B *et al.* 2020 Dissecting the sequence determinants for dephosphorylation by the catalytic subunits of phosphatases PP1 and PP2A. *Nat. Commun.* **11**, 3583. (doi:10.1038/s41467-020-17334-x)
23. Fowle H *et al.* 2021 PP2A/B55alpha substrate recruitment as defined by the retinoblastoma-related protein p107. *eLife* **10**, e63181. (doi:10.7554/eLife.63181)
24. Kruse T *et al.* 2020 Mechanisms of site-specific dephosphorylation and kinase opposition imposed by PP2A regulatory subunits. *EMBO J.* **39**, e103695. (doi:10.15252/embj.2019103695)
25. Hertz EPT, Kruse T, Davey NE, López-Méndez B, Sigurethsson JO, Montoya G, Olsen JV, Nilsson J. 2016 A conserved motif provides binding specificity to the PP2A-B56 phosphatase. *Mol. Cell.* **63**, 686–695. (doi:10.1016/j.molcel.2016.06.024)
26. Smith RJ, Cordeiro MH, Davey NE, Vallardi G, Ciliberto A, Gross F, Saurin AT. 2019 PP1 and PP2A use opposite phospho-dependencies to control distinct processes at the kinetochore. *Cell Rep.* **28**, 2206–2219. (doi:10.1016/j.celrep.2019.07.067)
27. Padi SKR, Godek RJ, Peti W, Page R. 2025 Cryo-EM structures of PP2A:B55 with p107 and Eya3 define substrate recruitment. *Nat. Struct. Mol. Biol.* **32**, 1373–1382. (doi:10.1038/s41594-025-01535-3)
28. Grallert A, Boke E, Hagting A, Hodgson B, Connolly Y, Griffiths JR, Smith DL, Pines J, Hagan IM. 2015 A PP1-PP2A phosphatase relay controls mitotic progression. *Nature* **517**, 94–98. (doi:10.1038/nature14019)
29. Nijenhuis W, Vallardi G, Teixeira A, Kops GJ, Saurin AT. 2014 Negative feedback at kinetochores underlies a responsive spindle checkpoint signal. *Nat. Cell Biol.* **16**, 1257–1264. (doi:10.1038/ncb3065)
30. Cho US, Xu W. 2007 Crystal structure of a protein phosphatase 2A heterotrimeric holoenzyme. *Nature* **445**, 53–57. (doi:10.1038/nature05351)
31. Xu Y, Chen Y, Zhang P, Jeffrey PD, Shi Y. 2008 Structure of a protein phosphatase 2A holoenzyme: insights into B55-mediated Tau dephosphorylation. *Mol. Cell* **31**, 873–885. (doi:10.1016/j.molcel.2008.08.006)
32. Vallardi G, Allan LA, Crozier L, Saurin AT. 2019 Division of labour between PP2A-B56 isoforms at the centromere and kinetochore. *eLife* **8**, e42619. (doi:10.7554/eLife.42619)
33. McCright B, Rivers AM, Audlin S, Virshup DM. 1996 The B56 family of protein phosphatase 2A (PP2A) regulatory subunits encodes differentiation-induced phosphoproteins that target PP2A to both nucleus and cytoplasm. *J. Biol. Chem.* **271**, 22081–22089. (doi:10.1074/jbc.271.36.22081)
34. Sandal P, Jong CJ, Merrill RA, Song J, Strack S. 2021 Protein phosphatase 2A - structure, function and role in neurodevelopmental disorders. *J. Cell Sci.* **134**, jcs248187. (doi:10.1242/jcs.248187)
35. Nasa I, Cressey LE, Kruse T, Hertz EPT, Gui J, Graves LM, Nilsson J, Kettenbach AN. 2020 Quantitative kinase and phosphatase profiling reveal that CDK1 phosphorylates PP2Ac to promote mitotic entry. *Sci. Signal* **13**, eaba7823. (doi:10.1126/scisignal.aba7823)
36. Mochida S, Ikeo S, Gannon J, Hunt T. 2009 Regulated activity of PP2A-B55 delta is crucial for controlling entry into and exit from mitosis in *Xenopus* egg extracts. *EMBO J.* **28**, 2777–2785. (doi:10.1038/emboj.2009.238)
37. Kamenz J, Gelens L, Ferrell JE, Jr. 2021 Bistable, biphasic regulation of PP2A-B55 accounts for the dynamics of mitotic substrate phosphorylation. *Curr. Biol.* **31**, 794–808. (doi:10.1016/j.cub.2020.11.058)
38. Kruse T, Zhang G, Larsen MS, Lischetti T, Streicher W, Kragh Nielsen T, Bjørn SP, Nilsson J. 2013 Direct binding between BubR1 and B56-PP2A phosphatase complexes regulate mitotic progression. *J. Cell Sci.* **126**, 1086–1092. (doi:10.1242/jcs.122481)
39. Kitajima TS, Sakuno T, Ishiguro K, Iemura S, Natsume T, Kawashima SA, Watanabe Y. 2006 Shugoshin collaborates with protein phosphatase 2A to protect cohesin. *Nature* **441**, 46–52. (doi:10.1038/nature04663)
40. Jiang W, Hallberg RL. 2000 Isolation and characterization of par1(+) and par2(+): two *Schizosaccharomyces pombe* genes encoding B′ subunits of protein phosphatase 2A. *Genetics* **154**, 1025–1038. (doi:10.1093/genetics/154.3.1025)

41. Chica N, Rozalen AE, Pérez-Hidalgo L, Rubio A, Novak B, Moreno S. 2016 Nutritional control of cell size by the greatwall-endosulfine-PP2A.B55 pathway. *Curr. Biol.* **26**, 319–330. (doi:10.1016/j.cub.2015.12.035)
42. Basu S, Greenwood J, Jones AW, Nurse P. 2022 Core control principles of the eukaryotic cell cycle. *Nature* **607**, 381–386. (doi:10.1038/s41586-022-04798-8)
43. Deng DJ, Wang X, Yue KY, Wang Y, Jin QW. 2022 Analysis of the potential role of fission yeast PP2A in spindle assembly checkpoint inactivation. *FASEB J.* **36**, e22524. (doi:10.1096/fj.202101884R)
44. Heidari B, Nemie-Feyissa D, Lillo C. 2023 Distinct clades of protein phosphatase 2A regulatory B′/B56 subunits engage in different physiological processes. *Int. J. Mol. Sci.* **24**, 12255. (doi:10.3390/ijms241512255)
45. Grallert A, Hagan IM. 2017 Large-scale immunoprecipitation from fission yeast cell extracts. *Cold Spring Harb. Protoc.* **2017**, 151–157. (doi:10.1101/pdb.prot091595)
46. den Elzen NR, O'Connell MJ. 2004 Recovery from DNA damage checkpoint arrest by PP1-mediated inhibition of Chk1. *EMBO J.* **23**, 908–918. (doi:10.1038/sj.emboj.7600105)
47. Ohkura H, Kinoshita N, Miyatani S, Toda T, Yanagida M. 1989 The fission yeast dis2+ gene required for chromosome disjoining encodes one of two putative type 1 protein phosphatases. *Cell* **57**, 997–1007. (doi:10.1016/0092-8674(89)90338-3)
48. Yamano H, Ishii K, Yanagida M. 1994 Phosphorylation of dis2 protein phosphatase at the C-terminal cdc2 consensus and its potential role in cell cycle regulation. *EMBO J.* **13**, 5310–5318. (doi:10.1002/j.1460-2075.1994.tb06865.x)
49. Songyang Z, Blechner S, Hoagland N, Hoekstra MF, Piwnica-Worms H, Cantley LC. 1994 Use of an oriented peptide library to determine the optimal substrates of protein kinases. *Curr. Biol.* **4**, 973–982. (doi:10.1016/s0960-9822(00)00221-9)
50. Mitchison JM, Nurse P. 1985 Growth in cell length in the fission yeast *Schizosaccharomyces pombe*. *J. Cell Sci.* **75**, 357–376. (doi:10.1242/jcs.75.1.357)
51. Hagan IM, Grallert A, Simanis V. 2016 cell cycle synchronization of *Schizosaccharomyces pombe* by centrifugal elutriation of small cells. *Cold Spring Harb. Protoc.* **2016**, pdb.prot091231. (doi:10.1101/pdb.prot091231)
52. Hiraoka Y, Toda T, Yanagida M. 1984 The NDA3 gene of fission yeast encodes beta-tubulin: a cold-sensitive *nda3* mutation reversibly blocks spindle formation and chromosome movement in mitosis. *Cell* **39**, 349–358. (doi:10.1016/0092-8674(84)90013-8)
53. Hagan IM, Grallert A, Simanis V. 2016 synchronizing progression of *Schizosaccharomyces pombe* cells from prophase through mitosis and into S phase with *nda3-KM311* arrest release. *Cold Spring Harb. Protoc.* **2016**, pdb.prot091256. (doi:10.1101/pdb.prot091256)
54. Singh P, Halova L, Hagan IM. 2021 Highly synchronous mitotic progression in *Schizosaccharomyces pombe* upon relief of transient Cdc2-asM17 inhibition. *Methods Mol. Biol.* **2329**, 123–142. (doi:10.1007/978-1-0716-1538-6_10)
55. Woods A, Sherwin T, Sasse R, MacRae TH, Baines AJ, Gull K. 1989 Definition of individual components within the cytoskeleton of *Trypanosoma brucei* by a library of monoclonal antibodies. *J. Cell Sci.* **93**, 491–500. (doi:10.1242/jcs.93.3.491)
56. Inoue R, Usui H, Tanabe O, Nishito Y, Shimizu M, Takeda M. 1999 Studies on functions of the 63-kDa A- and 74-kDa B′(delta)-regulatory subunits in human erythrocyte protein phosphatase 2A: dissociation and reassociation of the subunits. *J. Biochem.* **126**, 1127–1135. (doi:10.1093/oxfordjournals.jbchem.a022558)
57. Tanabe O, Nagase T, Murakami T, Nozaki H, Usui H, Nishito Y, Hayashi H, Kagamiyama H, Takeda M. 1996 Molecular cloning of a 74-kDa regulatory subunit (B" or delta) of human protein phosphatase 2A. *FEBS Lett.* **379**, 107–111. (doi:10.1016/0014-5793(95)01500-0)
58. Xu Z, Williams BR. 2000 The B56alpha regulatory subunit of protein phosphatase 2A is a target for regulation by double-stranded RNA-dependent protein kinase PKR. *Mol. Cell Biol.* **20**, 5285–5299. (doi:10.1128/MCB.20.14.5285-5299.2000)
59. Letourneux C, Rocher G, Porteu F. 2006 B56-containing PP2A dephosphorylate ERK and their activity is controlled by the early gene IEX-1 and ERK. *EMBO J.* **25**, 727–738. (doi:10.1038/sj.emboj.7600980)
60. Shouse GP, Nobumori Y, Panowicz MJ, Liu X. 2011 ATM-mediated phosphorylation activates the tumor-suppressive function of B56gamma-PP2A. *Oncogene* **30**, 3755–3765. (doi:10.1038/onc.2011.95)
61. Margolis SS *et al.* 2006 Role for the PP2A/B56delta phosphatase in regulating 14-3-3 release from Cdc25 to control mitosis. *Cell* **127**, 759–773. (doi:10.1016/j.cell.2006.10.035)
62. Usui H, Inoue R, Tanabe O, Nishito Y, Shimizu M, Hayashi H, Kagamiyama H, Takeda M. 1998 Activation of protein phosphatase 2A by cAMP-dependent protein kinase-catalyzed phosphorylation of the 74-kDa B″(delta) regulatory subunit in vitro and identification of the phosphorylation sites. *FEBS Lett.* **430**, 312–316. (doi:10.1016/s0014-5793(98)00684-x)
63. Ahn JH, McAvoy T, Rakhilin SV, Nishi A, Greengard P, Nairn AC. 2007 Protein kinase A activates protein phosphatase 2A by phosphorylation of the B56delta subunit. *Proc. Natl Acad. Sci. USA*. **104**, 2979–2984. (doi:10.1073/pnas.0611532104)
64. Dodge-Kafka KL, Bauman A, Mayer N, Henson E, Heredia L, Ahn J, McAvoy T, Nairn AC, Kapiloff MS. 2010 cAMP-stimulated protein phosphatase 2A activity associated with muscle A kinase-anchoring protein (mAKAP) signaling complexes inhibits the phosphorylation and activity of the cAMP-specific phosphodiesterase PDE4D3. *J. Biol. Chem.* **285**, 11078–11086. (doi:10.1074/jbc.M109.034868)
65. Wu CG *et al.* 2024 B56delta long-disordered arms form a dynamic PP2A regulation interface coupled with global allostery and Jordan's syndrome mutations. *Proc. Natl Acad. Sci. USA.* **121**, e2310727120. (doi:10.1073/pnas.2310727120)
66. Ahn JH, Kim Y, Kim HS, Greengard P, Nairn AC. 2011 Protein kinase C-dependent dephosphorylation of tyrosine hydroxylase requires the B56delta heterotrimeric form of protein phosphatase 2A. *PLoS ONE* **6**, e26292. (doi:10.1371/journal.pone.0026292)
67. Kirchhefer U, Heinick A, König S, Kristensen T, Müller FU, Seidl MD, Boknik P. 2014 Protein phosphatase 2A is regulated by protein kinase Calpha (PKCalpha)-dependent phosphorylation of its targeting subunit B56alpha at Ser41. *J. Biol. Chem.* **289**, 163–176. (doi:10.1074/jbc.M113.507996)
68. Janssens V, Goris J. 2001 Protein phosphatase 2A: a highly regulated family of serine/threonine phosphatases implicated in cell growth and signalling. *Biochem J.* **353**, 417–439. (doi:10.1042/0264-6021:3530417)
69. Hein JB, Garvanska DH, Nasa I, Kettenbach AN, Nilsson J. 2021 Coupling of Cdc20 inhibition and activation by BubR1. *J. Cell Biol.* **220**, e202012081. (doi:10.1083/jcb.202012081)
70. Tanabe O, Hirata D, Usui H, Nishito Y, Miyakawa T, Igarashi K, Takeda M. 2001 Fission yeast homologues of the B′ subunit of protein phosphatase 2A: multiple roles in mitotic cell division and functional interaction with calcineurin. *Genes Cells* **6**, 455–473. (doi:10.1046/j.1365-2443.2001.00429.x)
71. Fujimitsu K, Yamano H. 2020 PP2A-B56 binds to Apc1 and promotes Cdc20 association with the APC/C ubiquitin ligase in mitosis. *EMBO Rep.* **21**, e48503. (doi:10.15252/embr.201948503)
72. Quiniou M, Burns MC, McDermott A, Jaworek K, Scott SJ, Wakefield JG, Borgal L. 2025 The PP2A-B56 binding site LxxIxE contributes to Asp-mediated spindle pole stability. *Cytoskeleton (Hoboken)* **82**, 804–814. (doi:10.1002/cm.22013)

73. Espert A, Uluocak P, Bastos RN, Mangat D, Graab P, Gruneberg U. 2014 PP2A-B56 opposes Mps1 phosphorylation of Knl1 and thereby promotes spindle assembly checkpoint silencing. *J. Cell Biol.* **206**, 833–842. (doi:10.1083/jcb.201406109)
74. Foley EA, Maldonado M, Kapoor TM. 2011 Formation of stable attachments between kinetochores and microtubules depends on the B56-PP2A phosphatase. *Nat. Cell Biol.* **13**, 1265–1271. (doi:10.1038/ncb2327)
75. Ueki Y *et al.* 2021 A highly conserved pocket on PP2A-B56 is required for hSgo1 binding and cohesion protection during mitosis. *EMBO Rep.* **22**, e52295. (doi:10.15252/embr.202052295)
76. Chrupcala ML, Moseley JB. 2025 PP2A-B56 regulates Mid1 protein levels for proper cytokinesis in fission yeast. *Mol. Biol. Cell* **36**, ar52. (doi:10.1091/mbc.E24-08-0382)
77. Bernard P, Hardwick K, Javerzat JP. 1998 Fission yeast bub1 is a mitotic centromere protein essential for the spindle checkpoint and the preservation of correct ploidy through mitosis. *J. Cell Biol.* **143**, 1775–1787. (doi:10.1083/jcb.143.7.1775)
78. Bai S, Sun L, Wang X, Wang SM, Luo ZQ, Wang Y, Jin QW. 2022 Recovery from spindle checkpoint-mediated arrest requires a novel Dnt1-dependent APC/C activation mechanism. *PLoS Genet.* **18**, e1010397. (doi:10.1371/journal.pgen.1010397)
79. Akera T, Goto Y, Sato M, Yamamoto M, Watanabe Y. 2015 Mad1 promotes chromosome congression by anchoring a kinesin motor to the kinetochore. *Nat. Cell Biol.* **17**, 1124–1133. (doi:10.1038/ncb3219)
80. Niwa O. 2018 Determination of the frequency of minichromosome loss to assess chromosome stability in fission yeast. *Cold Spring Harb. Protoc.* **2018**, pdb.prot091991. (doi:10.1101/pdb.prot091991)
81. Jiang W, Hallberg RL. 2001 Correct regulation of the septation initiation network in *Schizosaccharomyces pombe* requires the activities of par1 and par2. *Genetics* **158**, 1413–1429. (doi:10.1093/genetics/158.4.1413)
82. Chica N, Portantier M, Nyquist-Andersen M, Espada-Burriel S, Lopez-Aviles S. 2022 Uncoupling of mitosis and cytokinesis upon a prolonged arrest in metaphase is influenced by protein phosphatases and mitotic transcription in fission yeast. *Front. Cell Dev. Biol.* **10**, 876810. (doi:10.3389/fcell.2022.876810)
83. Moreno S, Nurse P. 1994 Regulation of progression through the G1 phase of the cell cycle by the rum1+ gene. *Nature* **367**, 236–242. (doi:10.1038/367236a0)
84. Petersen J, Nurse P. 2007 TOR signalling regulates mitotic commitment through the stress MAP kinase pathway and the Polo and Cdc2 kinases. *Nat. Cell Biol.* **9**, 1263–1272. (doi:10.1038/ncb1646)
85. Suijkerbuijk SJ, Vleugel M, Teixeira A, Kops GJ. 2012 Integration of kinase and phosphatase activities by BUBR1 ensures formation of stable kinetochore-microtubule attachments. *Dev. Cell* **23**, 745–755. (doi:10.1016/j.devcel.2012.09.005)
86. Dohadwala M, da Cruz e Silva EF, Hall FL, Williams RT, Carbonaro-Hall DA, Nairn AC, Greengard P, Berndt N. 1994 Phosphorylation and inactivation of protein phosphatase 1 by cyclin-dependent kinases. *Proc. Natl Acad. Sci. USA* **91**, 6408–6412. (doi:10.1073/pnas.91.14.6408)
87. Kapadia N, Nurse P. 2025 Spatiotemporal orchestration of mitosis by cyclin-dependent kinase. *Nature* **643**, 1391–1399. (doi:10.1038/s41586-025-09172-y)
88. Allard CAH, Opalko HE, Liu KW, Medoh U, Moseley JB. 2018 Cell size-dependent regulation of Wee1 localization by Cdr2 cortical nodes. *J. Cell Biol.* **217**, 1589–1599. (doi:10.1083/jcb.201709171)
89. Le Goff X, Buvelot S, Salimova E, Guerry F, Schmidt S, Cueille N, Cano E, Simanis V. 2001 The protein phosphatase 2A B'-regulatory subunit par1p is implicated in regulation of the *S. pombe* septation initiation network. *FEBS Lett.* **508**, 136–142. (doi:10.1016/s0014-5793(01)03047-2)
90. Forester CM, Maddox J, Louis JV, Goris J, Virshup DM. 2007 Control of mitotic exit by PP2A regulation of Cdc25C and Cdk1. *Proc. Natl Acad. Sci. USA* **104**, 19867–19872. (doi:10.1073/pnas.0709879104)
91. Wolfe BA, Gould KL. 2004 Fission yeast Clp1p phosphatase affects G2/M transition and mitotic exit through Cdc25p inactivation. *EMBO J.* **23**, 919–929. (doi:10.1038/sj.emboj.7600103)
92. Wolfe BA, McDonald WH, Yates JR 3rd, Gould KL. 2006 Phospho-regulation of the Cdc14/Clp1 phosphatase delays late mitotic events in *S. pombe*. *Dev. Cell* **11**, 423–430. (doi:10.1016/j.devcel.2006.07.016)
93. Chan KY, Alonso-Nuñez M, Grallert A, Tanaka K, Connolly Y, Smith DL, Hagan IM. 2017 Dialogue between centrosomal entrance and exit scaffold pathways regulates mitotic commitment. *J. Cell Biol.* **216**, 2795–2812. (doi:10.1083/jcb.201702172)
94. Lin M, Xie SS, Chan KY. 2022 An updated view on the centrosome as a cell cycle regulator. *Cell Div.* **17**, 1. (doi:10.1186/s13008-022-00077-0)
95. Arquint C, Gabryjonczyk AM, Nigg EA. 2014 Centrosomes as signalling centres. *Phil. Trans. R. Soc. B.* **369**, 20130464. (doi:10.1098/rstb.2013.0464)
96. Lucena R, Alcaide-, Gavilán M, Anastasia SD, Kellogg DR. 2017 Wee1 and Cdc25 are controlled by conserved PP2A-dependent mechanisms in fission yeast. *Cell Cycle* **16**, 428–435. (doi:10.1080/15384101.2017.1281476)
97. Fennessy D *et al.* 2014 Extending the *Schizosaccharomyces pombe* molecular genetic toolbox. *PLoS ONE* **9**, e97683. (doi:10.1371/journal.pone.0097683)
98. Bähler J, Wu JQ, Longtine MS, Shah NG, McKenzie 3rd A, Steever AB, Wach A, Philippsen P, Pringle JR. 1998 Heterologous modules for efficient and versatile PCR-based gene targeting in *Schizosaccharomyces pombe*. *Yeast* **14**, 943–951. (doi:10.1002/(SICI)1097-0061(199807)14:10<943::AID-YEA292>3.0.CO;2-Y)
99. Gibson DG, Young L, Chuang RY, Venter JC, Smith HO. 2009 Enzymatic assembly of DNA molecules up to several hundred kilobases. *Nat. Methods* **6**, 343–345. (doi:10.1038/nmeth.1318)
100. Grallert A, Hagan IM. 2017 Small-scale immunoprecipitation from fission yeast cell extracts. *Cold Spring Harb. Protoc.* **2017**, pdb.prot091587. (doi:10.1101/pdb.prot091587)
101. Hagan IM. 2016 Chromatin and cell wall staining of *Schizosaccharomyces pombe*. *Cold Spring Harb. Protoc.* **2016**, pdb.prot091025. (doi:10.1101/pdb.prot091025)
102. Hagan IM. 2016 Immunofluorescence microscopy of *Schizosaccharomyces pombe* using chemical fixation. *Cold Spring Harb. Protoc.* **2016**, pdb.prot091017. (doi:10.1101/pdb.prot091017)
103. Hagan IM, Grallert A, Simanis V. 2016 Synchronizing progression of *Schizosaccharomyces pombe* cells from G2 through repeated rounds of mitosis and S phase with cdc25-22 arrest release. *Cold Spring Harb. Protoc.* **2016**, pdb.prot091264. (doi:10.1101/pdb.prot091264)
104. Booher RN, Alfa CE, Hyams JS, Beach DH. 1989 The fission yeast cdc2/cdc13/suc1 protein kinase: regulation of catalytic activity and nuclear localization. *Cell* **58**, 485–497. (doi:10.1016/0092-8674(89)90429-7)
105. Petersen J, Russell P. 2016 Growth and the environment of *Schizosaccharomyces pombe*. *Cold Spring Harb. Protoc.* **2016**, pdb top079764. (doi:10.1101/pdb.top079764)
106. Halova L, Connolly Y, Smith D, Petersen J, Hagan I. 2026 Supplementary material from: CDK1-Cyclin B mediated phosphorylation of PP2A-B56 on B56Par1 .T73T75 controls mitotic entry timing and *Schizosaccharomyces pombe* cell size. Figshare. (doi:10.6084/m9.figshare.c.8576140)